Combining Remote Sensing and Techniques for Rainfall Runoff Modelling and Flash Flood Mapping in the UAE

Benhur Kessete Asefaw

MSc. Thesis

November 2020

A thesis submitted to Khalifa University of Science and Technology in accordance with the requirements of the degree of Master of Science in Water and Environmental Engineering in the Department of Civil Infrastructure and Environmental Engineering.

Combining Remote Sensing and Techniques for Rainfall Runoff Modelling and Flash Flood Mapping in the UAE

by

Benhur Kessete Asefaw

A thesis submitted in partial fulfillment of the requirements for the degree of

MSc in Water and Environmental Engineering

at

Khalifa University

Thesis Committee

Dr. Annalisa Molini (Advisor),
Khalifa University

Dr. Marouane Temimi (External Advisor),
Stevens Institute of Technology

Dr. Michele Lanotte (RSC member),
Khalifa University

Dr. Mariam R. Al Shehhi (RSC member),
Khalifa University

November 2020

Abstract

Benhur Kessete Asefaw, "**Combining Remote Sensing and Techniques for Rainfall Runoff Modelling and Flash Flood Mapping in the UAE**", M.Sc. Thesis, MSc in Water and Environmental Engineering, Department of Civil Infrastructure and Environmental Engineering, Khalifa University of Science and Technology, United Arab Emirates, November 2020.

This research work focused on preparation of a continuous hydrological based model to monitor the variability of surface runoff and subsequently to prepare flash flood maps using remote sensing and modelling mechanism. The study case is the wadi Ham in the North eastern part of the United Arab Emirates (UAE). Phase one of the project involved the rainfall-runoff modelling of Wadi Ham in a continuous, distributed modelling approach. Hydrologic Engineering Centre Hydrological Modelling System (HEC-HMS) was adapted as the simulating model. The bulk precipitation data obtained from Global Precipitation Measurement (GPM) mission (1 day, 0.1^0 product) was automatically imported to HEC-HMS after specifying various parameters such as soil property, temperature and routing method for the runoff. After running the model, simulated runoff hydrographs and volume at the outlet section (Ham/Fujairah Dam) were generated. Area of Imperviousness was found to be sensitive. After calibrating the model using this variable, a significant similarity result (only 8% difference) was observed between the estimated and observed volume for the March 13, 2016 event. Landsat-8 images were used to extract the observed area of the water body. With 2% of the basin area impervious, the model gave a relatively smaller difference (RMSE of 0.24) for all events considered between the simulated and the observed volume of water at the reservoir.

The second phase comprises the hydraulic simulation and generation of flash flood maps within the wadi basin. The simulated and validated maximum runoff hydrographs obtained in the hydrologic model (first phase) were used to perform 2D hydraulic modelling in Hydrologic Engineering Centre River Analysis System (HEC-RAS). Moderate Resolution Imaging Spectroradiometer (MODIS) land cover of the area (daily, 0.5km product) was used in specifying the manning roughness coefficient based up on the type of the land cover. Flood hazard maps and maximum water depth profiles at various sections were finally prepared after the defining the boundary conditions. These hydrologic and hydraulic simulated results gave an insight and are expected to contribute to an improved managerial system in water resources and also in identifying flash flood vulnerable areas during similar magnitude rainfall events in that area of the UAE. As a recommendation, and for the adapted hydraulic model to be used efficiently, a very fine resolution, 10 m or less, digital elevation model (DEM) with cloud free satellite images of the wadi during floods are necessary. These simulation models performed can play an important role in the direct assessment of the impact of future developments on the surface and subsurface water dynamics, and increasing in the national water storage capacity as per the UAE water security strategy 2036.

Key words: Flood map, GPM, Hydrologic modelling, HEC-HMS, HEC-RAS, Landsat, Wadi Ham.

Acknowledgement

First and for most, I would like to thank the Almighty God for His Grace and Blessings and allowing me to stay healthy and focused to complete this thesis paper which is part of my long term dream to achieve a Master's degree in Engineering.

I want to use this opportunity to extend my appreciation to Khalifa university for providing the scholarship and the support throughout the study period.

Special thanks goes to my supervisor Dr. **Annalisa Molini**, for her unfailing cooperation and sparing her valuable time especially during the start of the project and assisting me in getting data and valuable information from a to z of the project.

Special thanks also goes to Dr. **Marouane Temimi,** former advisor and later on External advisor, for his relentless support through the study period. In this time his regular review of the paper, constructive comments and inspiration throughout my work really helped me a lot. The guidance and encouragement when I feel desperate and understanding and insightful support throughout the project work was owing. Thank you Professor.

I am also thankful to the RSC members of my project Dr. **Michele Lanotte** and Dr. **Mariam R. Al Shehhi** for their helpful suggestions, and supports in providing valuable information and opening opportunities for me to get in touch with other professors during the study period. Special thanks also goes to Dr. **Alessandro Decarlis** from Earth Science department in providing me information regarding the geology of the study area. I also want to extend my thanks to Dr. **Ricardo Morais Fonseca**, a research scientist, who has helped with the editing and gave scientific comments.

Above ground, I am greatly indebted to my family (Dad, Mom, and my beloved sisters), whose value to me only grows with age, for their unconditional support, love and believe on me no matter where. And finally, a special acknowledgement my dearest wife and best friend, **Nazret**, my champion, for her relentless support, motivation, and patience till the completion of this thesis paper.

Last but not least, it is with immense and heartfelt gratitude and respect; I would like to extend my thanks to my dear friends, colleagues and others whose names are not mentioned in this acknowledgment for their support and encouragement in the completion of this thesis paper.

Benhur Kessete Asefaw

Declaration and Copyright

Declaration

I declare that the work in this thesis was carried out in accordance with the regulations of Khalifa University of Science and Technology. The work is entirely my own except where indicated by special reference in the text. Any views expressed in the thesis are those of the author and in no way represent those of Khalifa University of Science and Technology. No part of the thesis has been presented to any other university for any degree.

Author Name: Benhur Kessete Asefaw

Author Signature: 

Date: November 2020

Copyright ©

Contents

List of Tables

List of Figures

List of Abbreviations

DEM	*Digital Elevation Model*
EFDC	*Environmental Fluid Dynamics Code*
EVI	*Enhanced Vegetation Index*
FAO	*Food and Agriculture organization*
FLUCOMP	*Fluid Computation*
GPM-IMERG	*Global precipitation measurement Integrated Multi-SatellitE Retrievals for GPM*
HEC-DSS	*Hydrologic Engineering Center-Digital storage system*
HEC-GEOHMS	*Hydrologic Engineering Center-Geospatial Hydrologic Modeling Extension*
HEC-HMS	*Hydrologic Engineering Center-Hydrologic Modelling System*
HEC-RAS	*Hydrologic Engineering Center-River Analysis System*
JAXA	*Japan Aerospace Exploration Agency*
MNDWI	*Modified normalized difference water index*
MODIS	*Moderate Resolution Imaging Spectroradiometer*
MSWEP	*Multi-Source Weighted-Ensemble Precipitation*
NASA	*National Aeronautics and Space Administration*
NDWI	*Normalized difference water index*
NGA	*National Geospatial-Intelligence Agency*
OLI	*Operational Land Imager*
SRTM	*Shuttle Radar Tropical Meteorology*
TIRS	*Thermal Infrared Sensor*
TRMM	*Tropical rainfall measuring Mission*
USGS	*United states for Geological survey*
WASH123D	*WAterSHed Systems of 1-D Stream-River Network, 2-D Overland Regime, and 3-D Subsurface Media*
WSE	*Water surface elevation*

Chapter 1

1. Introduction

1.1. The UAE and Water Resources

The United Arab Emirates is located in the southeast part of the Arabian Peninsula, between 22º40'N and 26º00'N latitude and 51º00'E and 56º00'E longitude. It has an area of around 83,600 $km^2$and is bounded by the Kingdom of Saudi Arabia to the west and south, the Sea of Oman and Oman on the east and northeast and the Arabian Gulf to the north. The UAE is mostly flat, except over eastern and northeastern parts where the Al Hajar mountains rise to more than 2,000 m above ground level [1]. The low lying zone ranges from sea level to a height of 300m and characterized by sand dunes. The mountainous zone is comprised of isolated anticlinal hills and mountains run on north south directions. Jabal Bil Ays is the highest mountain in this region reaching 1934m above sea level.

The UAE is located in the arid zone. It has a long hot summer and short mild winter. According to Ministry of Agriculture and Fishery's report [2], the mean annual temperature is around 30^0C ranging from 14^0C in winter to more than 45^0C in summer [3]. Relative humidity is higher in coastal area compared to the interior. In the winter, the mean relative humidity is around 60% and reaches around 50% in the summer. The range of the annual evapotranspiration is from 80mm to peak values of 2200mm [4]. Despite to the short and small-scale local (orographic) convective events occurring in the eastern part of the country during the summer time, most of the sporadic rainfall usually falls in the winter season with maximum intensity in the months of February and March [5], [6]. The annual precipitation totals vary from about 40 mm in the southern desert to 160 mm in the Al Hajar mountains [7]. RAD fog is common in flat and desert areas such as UAE. It occurs in clear sky condition as a result of frequent occurrence of nocturnal inversions promoting condensation or the super-saturation of the surface radiative cooling [8], [9].

Water is the cornerstone for the social and economic development of a society. Reliable water supply is a key factor for the survivability of mankind. Moreover, water is also an essential entity for ensuring the integrity of the Earth's ecosystems. According to the United States Geological Survey [10], 97% of the total earth's water is salt water, which is found in the oceans. Only the remaining 3% is fresh water. From this fresh water, two third exist in the form of ice in the polar areas and mountainous regions. Less than 2% of this fresh water is available on the surface in lakes and streams. Arid or semi-arid regions of the world cover almost 33% of the Earth's surface. These regions are called arid zones, since they possess dry climate with almost no rainfall but very high annual evaporation rates. They also experience deficiency in rather dry soils which is unfavorable to farming practices. In contrast, the scarce and sporadic rainfall is, at times, rather heavy [11], which can led to flash flooding. In this century, the water crisis become noticeable in arid and semi-arid regions where the drought conditions prevail [12]. According to statistical analysis, in the past one and half century, the world's total population has increased four times, and is also predicted to double in the coming three to four decades. Hence, from this statistical report the projected population, five billion people will live in countries experiencing moderate or severe water stress by the year 2025 [13], [14], [15]. This increase in population, higher living standards and industrialization are causing additional stress in the available fresh water resources which are becoming depleted. Thus, an efficient water management is required, which can be achieved through a better understanding of the hydrologic process in arid and semi-arid areas [16].

Due to the limited freshwater resource in the UAE, and the rapid increase of population, water demand has increased abruptly in the last three decades. The UAE is relying more on non-conventional water resource such as the desalinated water and treated waste water [17]. Most part of the freshwater demand for drinking is met through desalinated water. The treated water is mainly used in landscaping and forestry developments. Seasonal floods, springs and groundwater are the major conventional water resources in the country. However, surface water is very limited for direct utilization. On the other hand, ground water, which is depleting this time, is the vital natural source of freshwater for drinking and irrigation [18]. For regions like the UAE, Cloud seeding for rain enhancement offers a potential in ensuring a sustainable water supplies [19]. This operation is in practice for the past three decades. The low rate of rainfall and high evaporation rates makes the surface water, conventional resource, to be limited. As a result, there are no perennial rivers and lakes in the country. Seasonal flood called wadi, springs and falajes exist in the eastern and northern part of the country due to the intense but short duration rain storms [17].

Chapter 2

2. Objectives and Goals

Any rainfall runoff studies, such as floods, require hydrographs for imaginary events with specific return periods, generated with hydrologic models of single event type. Studies of wadi/river stability and ecology require investigation of the entire variety of wadi/river flows, as represented by the discharge versus time (known as flow-duration curve). A continuous hydrologic simulation model is the suitable tool for such studies. The main goal of this project is to monitor the variability of surface runoff in the wadi Ham located in the northeast part of the UAE in a continuous way using remotely sensed gridded precipitation data in a distributed hydrological model. The conceptual frame work of the thesis and the modelling processes is shown in *Figure 2-1*.

The specific objectives of the study include:

a. To assess the use of satellite driven product, GPM, in hydrological modeling.
b. To identify the geometrical, hydrological, and hydrogeological characteristics of the wadi Ham basin including catchment boundary and area, drainage stream pattern, precipitation (gridded), basin parameters, infiltration rates (based on the soil type) and evaporation rates.
c. To adapt hydrological modelling tool (HEC-HMS) of runoff using remote-sensed data to show the variability of surface runoff and able to simulate it.
d. To adapt hydraulic modelling tool (HEC-RAS) of runoff. This will help in generating flood maps to be used in identifying the flood prone areas within the wadi Ham basin.
e. To implement such hydrologic and hydraulic models in other wadis with similar geomorphology and climate characteristics.

As precipitation is the main component of hydrological models, water resources heavily depend on it. However, the current ground-based precipitation measuring devices, such as rain gauges, are very sparse and do not provide even distribution of the rainfall. Therefore, remote-sensed gridded precipitation data obtained from GPM mission at a 1 day temporal and 0.1^0 spatial resolution will

be applied in this study. This is expected to deliver the exact value of precipitation spatially. It is evident that weather radars generate high resolution estimates of rainfall above the surface by emitting electromagnetic radiation and collecting the echo (or the backscatter) despite to the fact that they produce range dependent errors and their high maintenance cost [20], [21]. However, satellites offer technology capable of providing extensive measurements of rainfall in real time over wide areas on a global scale. These include the Climate Research Unit (CRU) [22], Climate Prediction Center morphing (CMORPH) [23], Precipitation Estimation from Remotely Sensed Information using Artificial Neural Networks (PERSIANN) [24], the Global Precipitation Climate Center (GPCC) [25], and the Global Precipitation Measurement (GPM) [26], which is the successor of the Tropical Rainfall Measurement Mission (TRMM) [27]. These technologically-advanced satellite driven products can provide measurements of the reflectivity of the target hydrometeors after being interpreted. In addition, there are significant quality-control problems which have to be dealt with, such as the removal of ground mess or disorder [21]. Satellite-based products have shown uncertainty throughout the world [28]. They seem to be time and space sensitive, as their reliability varies over different regions and during different seasons. This creates a potential bias in water resource assessments and investigations when integrating such products in hydrological models or studies. Fekete et al. [29] stated that there is a larger disagreement between satellite-derived rainfall estimates and in-situ measurements from rain gauges in arid regions compared to mid-latitude regions in the world. So far, the assessment of these remotely sensed precipitation products was rarely performed over arid and semi-arid regions, even though arid areas cover almost 25% of the world. It is this reason that Fekete et al. [29] stated, “precipitation estimates over arid and semi-arid areas require significant improvements”. Precipitation and runoff have a nonlinear relationship as such the uncertainty in estimating precipitation causes a substantial change in the hydrologic processes. Yang and Luo [30] performed a study on the reliability of the satellite based products on the arid region of northwest China and found that the PERSIANN and the CMORPH products overestimated the precipitation. On the other hand, the TRMM daily product performed relatively better with acceptable precision even though they suggested applying a correction factor before using it. Similar suggestions were also made by Almazroui [31] for the precipitation records over Saudi Arabia. Wehbe et al. [28] also proposed a correction factor for the TRMM records over the UAE after comparing it with other products. GPM-IMERG, which is the successor of TRMM was tested for its accuracy in the UAE. From the results of Mahmoud et al. [32], the final-run-product of GPM showed the highest detection of precipitation with a lower estimation error when compared with the local ground based rain gauges. Wehbe et al. [6] also revealed that the GPM estimates recorded a higher Pearson correlation coefficient in the northeastern highlands of UAE.

From their finding, satellite precipitation records show much less bias in areas with geographically high altitude and higher precipitation rates.

To the knowledge of the author, this project is the first to conduct hydrological modelling using remotely sensed precipitation data and subsequently prepare the flood hazard maps. These maps will be used to identify the vulnerable area during the flash flooding within the basin. This is a crucial step in developing a better water management plan, and also in understanding the consequences of extreme hydrologic events.

2.1. Limitation of the study

The hydrologic analysis is performed using rainfall data, geographic information of the area, soil type, and vegetation cover to generate runoff flow and volumes at the outlet section in HEC-HMS. According to the reports documented by Ministry of Agriculture and forestry [2], the northeastern watershed experiences flash flooding from intense but short rainfall events. The flood flow takes place during the winter season in the months of February and March. In this area, there is no any stream flow gauging stations for measuring the flow/discharge using the rating curve process or stage-discharge curve in the past 30 years. It is documented that the installed gauging stations at specific locations within the Ham basin were destroyed by flash flooding in the early 1990s and have not been replaced yet. This is one of the main limitation of the work and was an obstacle in forecasting runoff. The second limitation is the unavailability of a recent DEM (from the year 2014 onwards) with spatial resolution less than 10m. Hence, the flood inundation map in the city of Fujairah and the effect of the short but intense rainfall creating flash floods passing through the built up area could not be clearly shown in the simulation as the adopted hydraulic model was significantly affected. Had the DEM used been at finer resolution, the impact/effect of the flash flood in the built up area would have been seen in the simulation model.

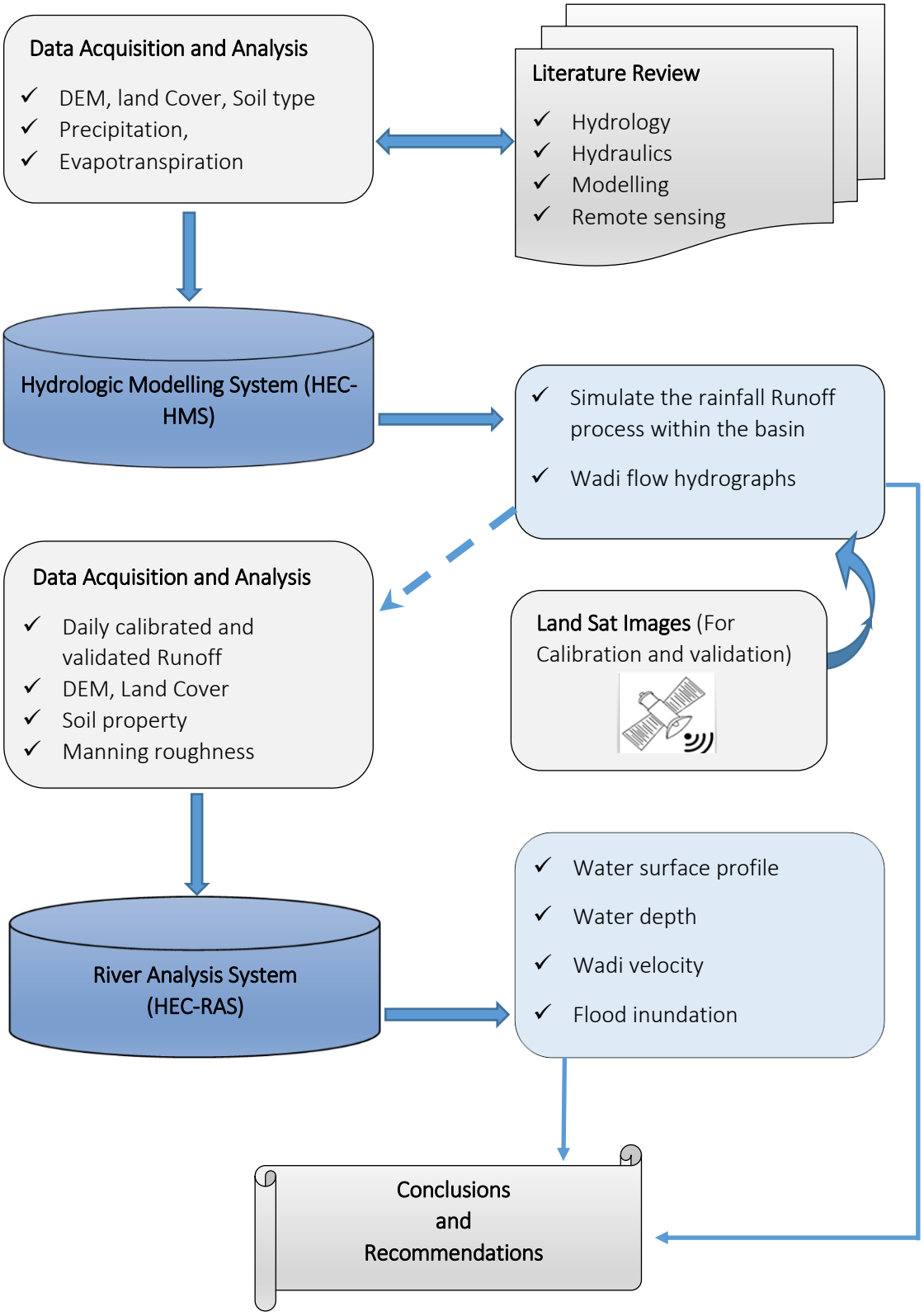

Figure 2-1: Conceptual Framework of the thesis and Modelling Processes

Phase 1

Hydrologic Modelling

Chapter 3

3. Hydrological Modelling

3.1. Hydrological models

Hydrological models are the basic illustrations of the actual hydrological cycle used to aid in providing viable solutions for integrated water resources planning and management. Based on the capabilities and limitations, hydrologic models are classified in two categories [33].

1) Physically based model: mathematically idealized representation of real phenomena, includes the physical process of the catchment [34]. This physical model is sub classified in two: scale and analog models.
   a) Scale model: the physical representation of the real system,
   b) Analog model: is based on equivalent ways to represent the process. For instance, the flow principle of electricity and that of water is the same.
2) Mathematical models: logical programming languages are used to develop these models and concepts, and explain the land phase of the hydrological cycle both spatially and temporally [35].

According to [33] and [36], a mathematical model is classified as stochastic and deterministic.

i. Stochastic models: different values of output can be produced for a single set of input that have some randomness.
ii. Deterministic models: the relationship among states and events are the determinant factors for the outcomes, without consideration of random variation. In other words, the deterministic model will produce the same output for a single input value without accounting randomness. Deterministic models are further divided into three broad categories namely lumped, distributed, and semi-distributed models [37].

a. Lumped models: treat the catchment as a whole (unit), with state variables representing the averages over the entire basin [38]. However, in [39] findings, land use and the spatial variability of the hydrological process are not accounted for lumped models.
b. Distributed models: divide the catchment into grid net (or cells) and flows are passed from one node (cell) to another as water drains through the basin. These models have state variables that represent local averages just like the lumped ones [40]. They require an extensive amount of data for parameterization [41].
c. Semi-distributed model: partly accounts for variations in space, with the division of the catchment into sub-basins. This model has some advantages of both types of spatial representation. This type of model category is further divided into event and continuous based hydrological models. Event-based models are usually for a single hydrological event of relatively short period of time (e.g. storm, flood), whereas continuous-based hydrological models simulate multiple state variables (e.g. soil moisture, surface storage) for a longer period.

The Hydrologic Engineering Center Hydrologic Modelling System (HEC-HMS), developed by the US Army Corps of Engineers, is a physically based and deterministic model. The elements of this model are arranged in a dendritic network, a pattern which looks like the branching of tree roots, and an upstream to downstream sequence is followed for the computational analysis [42]. This system comprises losses, transformation of rainfall to runoff, routing of the generated flow, analysis and rainfall-runoff simulation, and parameterization of variables. HEC-HMS has been used for a variety of purposes, including flood forecasting [43], storm water management [44], and climate impact assessment [45]. In HEC-HMS both continuous and event-based hydrological phenomena can be simulated. The event-based simulation is used for rainfall-runoff processes resulting from a single storm on modelling direct runoff hydrograph or peak discharge. However, continuous-based simulation allows you to model for long period of time, from months to years which allows a continuous accounting of the water stored in the basin. The primary difference is that both evapotranspiration and groundwater seepage flow are neglected in event-based modeling. In HEC-HMS, there are many methods listed for the loss method. In continuous based modelling where the model is gridded one, the Hamon Method [46] is one of the methods adopted where the loss through evapotranspiration is considered. In a continuous-based model, precipitation is taken as its input and routes it through the canopy, and then surface water storage. Recently, there have been advancements in computing technology and this led to the proper utilization of the dynamic routing

models in flood forecasting [47]. Likewise, HEC-HMS was implemented to predict reservoir inflow along the Red river in North Dakota and Minnesota by the US Army Corps of Engineers, which is considered as one of the main applications of this model [48]. Hu et al. [48] also found that this kind of models provided reasonable streamflow simulations for a range of soil moisture conditions. Likewise, in this arid region, [49] used HEC-HMS for the rainfall runoff analysis using the ground-based precipitation data on a continuous base in a distributed model. Considering the merits of using the satellite-based measurements and their reliability and consistency as per the studies performed by several researchers [6], [28], and [32] for the northeastern highlands of the UAE, this paper mainly focus on the preparation of a continuous hydrological simulation model in a distributed manner using remote-sensed data. Studies of flooding, stream stability and stream ecology require different types of hydrologic information. This type of hydrologic model generated a continuous record of stream/wadi flow from records of rainfall and other climatic variables.

3.2. Study Area

The UAE terrain comprises mountains, sand dunes, coastal plains, and drainage basins. The land in the UAE is a mixture of variety of soil textures (such as clay, coarse sand, clay loam, loam, fine sandy loam, sandy clay, silty, fine sand, loamy sand, sand, silty clay and silt) [50]. Furthermore, the soil is categorized as wet, humid, dry and very dry in relation to soil moisture [3]. The land slope is not a critical factor in the UAE, as more than 90% of the land has a slope less than 5%. The elevation of the land ranges from sea level to 1934 m above sea-level. The area is mainly made up of a rugged, upland massif rising to around 1000 m above datum, and forming part of the Al Hajar Mountain chain. The mountains fall steeply eastward to a narrow (1 to 6000m wide) coastal plain. In the west, the mountains descend onto desert gravel plains stretching to the Arabian Gulf. They are transected by a number of deeply incised northeast trending valleys, of which wadi Ham is the largest [51]. The major study area in this thesis is the watershed of wadi Ham as shown in *Figure 3-1*. From the central watershed of the Al Hajar Mountains, the southeast flowing wadi Ham and its tributaries dominate the eastern drainage pattern. West of the watershed, several wadi systems drain into the thick quaternary deposits of the western plains. The coastal plain is dominated by the large alluvial fan at the mouth of wadi Ham that provides the main aquifer supplying water to Fujairah city.

The climate of the study area is arid, with sparse, sporadic and unpredictable winter rainfall. Daily maximum and minimum temperatures vary from 24/16°C in January to 45/32°C in June [52]. Consequently, the vegetation is sparse, consisting of acacia scrub on the coastal plain, and low spiny bushes (including euphorbia species) in the mountains, the summits of which are slightly more

luxuriant, in part due to rare periods of mist. Some larger wadis like wadi Ham also contain large Sidr trees in addition to acacias. Although the UAE does not have any perennial streams, there are wadis, which are dry most of the year. Yet large volume of water is drained through these wadis from a short duration but intense rainfall [11], [53], [54]. According to Sheriff et al. [55], more than 50% of the annual rainfall occurs in February and March. As a result of the water runoff, the so called flash flooding mostly occurs in those months. Wadi Ham is one of the main wadis located in the Fujairah Emirates flowing from the Masafi highlands with over 1100m towards the southeast and draining towards the Gulf of Oman as shown in *Figure 3-1*. The soil type in this area is mostly covered by torriorthents [56]. These have more than 35% by volume gravel in the alluvial fans and plains adjacent to the mountains and throughout the wadi profile. The texture of these types are sandy and loam soil. They are considered to be of limited suitability for irrigated agriculture and very pervious due to their gravel content.

Wadi Ham is the path of the runoff from the mountains of Massafi to the lowlands of the Fujairah. Water is collected in the Ham dam's reservoir located at the end of the wadi before reaching the city of Fujairah. The Ham dam, which is a rock fill structure constructed in 1982, is located in the Fujairah emirate. The dam's reservoir has the capacity to hold up to 7.8 million cubic meters of water. The maximum height of the dam is 16 m and 2800 m long [57].

The total area of the drainage network (watershed) of this wadi is 193 km^2 as per the calculated area of the delineated watershed from the DEM in ArcGIS. The climate of this area is hyper arid with an average rainfall of 80mm per year [58]. The wet and dry seasons are winter (Dec, Jan and Feb) and summer (between May and September), respectively. Despite the long dry season but short duration flooding, Sheriff et al. [49] revealed that there is no practice of farming activities in the periphery of this wadi. However, there is scarce and sparse vegetation. The DEM retrieved from the Shuttle Radar Topography Mission (SRTM), shows the range of the elevation of this basin from 42 m to 1112 m as shown in *Figure 3-2*. This main drainage network is somehow mountainous, and water is collected at the lower land where the Dam is built not just to recharge the groundwater but also to act as a shield, preventing the city of Fujairah from flash floods generated from the mountainous area.

In the Al-Rawas and Valeo [59] study, the topography, geology and rainfall in arid regions such as the UAE tends to result in a highly non-linear runoff generation process. As most wadis are generated from the mountainous northeastern part of the country and Oman, runoff is generated during high intensity but short duration storms on bare land. This could infiltrate and recharge the local aquifers. But most importantly, this short duration but very intense rainfall generates a surface

runoff (flash flooding) directed to the lowland area. The rainfall characteristics (the intensity and duration) behaves different not only from region to region but also from basin to basin or sub-basin for the same catchment area. From a hydrological perspective, flooding is created as a result of heavy rainfall at higher altitudes. Likewise, in this wadi, most of the rainfall in the mountainous area drains towards the lower plain and coastal area as runoff. However, on an annual basis, and due to the high evapotranspiration rate which sometimes reaches up to 2200mm [4] and high percolation, the expected runoff volume is almost inexistent at the outlet of the wadi. This idea or notion is supported by studies performed in several parts of the world [60], [61], [62], [63], and [64].

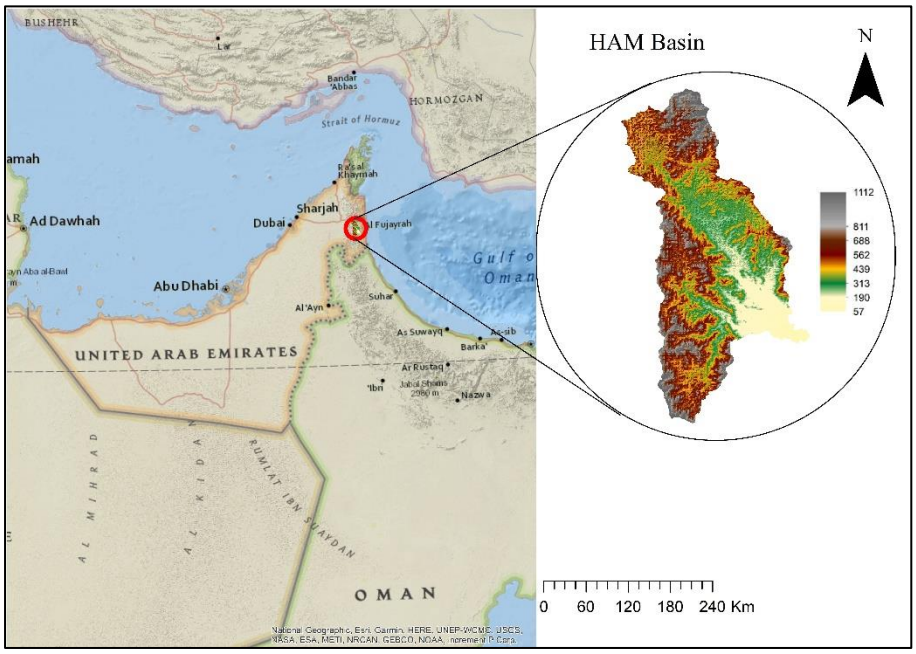

Figure 3-1*: Location of Ham basin in the UAE; Color bar used for the showing elevation range from the DEM*

This paper mainly focuses on the development of hydrological modelling of runoff using remote-sensed precipitation data as the main input. Studies performed by [6], [28], and [32] stressed that using satellite-derived precipitation data (TRMM/GPM) specifically in the chosen study area for the hydrological modelling is beneficial to manage the water resources.

3.3. Observational Datasets

The observational datasets used on the study include precipitation, DEM, and waterbody images obtained from the GPM, SRTM and Landsat Satellites, respectively. Other input datasets, such as soil and land use layers, were from the global FAO website. SRTM was used to obtain the DEM of the Ham watershed [65]. This dataset is at a spatial resolution of 30 m, with global coverage. The SRTM satellite works on a single pass interferometry, which makes use of two signals at the

same time from two different antennas of a radar. The surface elevation of the area is calculated by taking the difference of these signals. This product is developed by NASA (National Aeronautics and Space Administration) and the NGA (National Geospatial-Intelligence Agency), and has a geographic projection with WGS84, approximate definition of sea level, as horizontal datum reference. It is freely available online on the NASA reverb or USGS Earth Explorer. In ArcMap with HEC-GEOHMS as an extension, the watershed boundary delineation and stream network development are done using the DEM. The developed stream network is in a cascade manner from one pixel to another. As such, the water collected in pixels of higher elevation flows to those of lower elevation. The *Figure 3-2* shows the DEM of the HAM watershed.

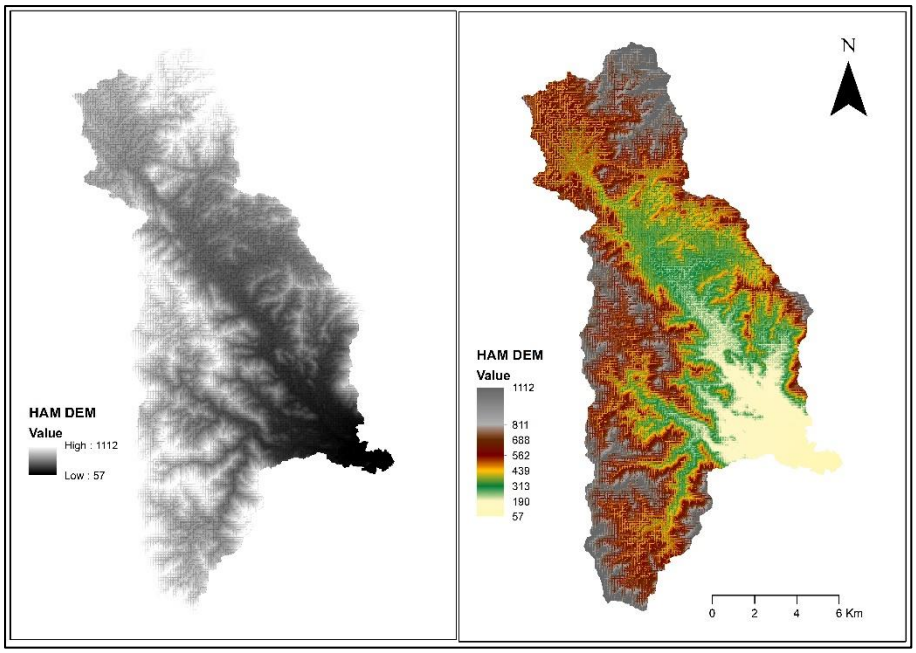

Figure 3-2: Both left and right (colored) indicates the elevation range (unit in meters) of the Ham basin from the DEM.

The precipitation measurements were retrieved or extracted from the Global Precipitation Measurement-Integrated Multi-SatellitE Retrievals (GPM-IMERG). GPM is the network of satellites providing the next-generation observation of rainfall and snow. This is developed by National Aeronautics and Space Administration (NASA) and Japan Aerospace Exploration Agency (JAXA), succeeding TRMM in 2013. This mission helps in the level of understanding the Earth's water cycle and improved forecasting schemes for extreme events. The algorithm of GPM-IMERG is meant to calibrate, merge, and interpolate all satellite microwave precipitation estimates, together with microwave-calibrated infrared (IR) satellite estimates, precipitation gauge analyses, and potentially other precipitation estimators at fine spatial and temporal scales for the TRMM and GPM eras over the entire globe [66]. GPM has a higher temporal (every 30 minutes) and spatial resolution (0.1°×0.1° roughly 10km×10km) compared to other satellites. The three GPM satellite

products (early, late and final run) have different characteristics. The near real-time products with a latency of 4 hours and 12 hours are early and late run, respectively. Generally, these products are intended to help scientists predict the impact of large storm events. While the last product of the GPM, called the final run product, is a reprocessed and gauged-adjusted product, providing a much higher latency of 2.5months and designed to be used for scientific research purposes. The main focus of GPM's core observation is on heavy to moderate rainfall on tropical and subtropical regions. Moreover, light rainfall (less than 0.5mm per hour) can also be observed through GPM. This makes precipitation measured by GPM preferable to be used as fractions of rainfall can also be recorded in this hyper-arid region.

Although the UAE lies in an arid region with a shortage of rainfall, the country's future plans mainly focus on the rainfall enhancement (such as rain seeding) [19], with an accurate monitoring and assessement of the rainfall runoff system to guarantee an efficient management of its water resources. The sporadic nature of the rainfall events, along with its substantial temporal and spatial variation, has increased the challenge of the monitoring and assessing rainfall across the UAE. Hence, to enhance and manage rainfall resources and prepare risk mitigation plans to protect lives and properties from the effects of flash floods, an understanding of the pattern of rainfall variability in the UAE is vital. To get an accurate and representative precipitation value of the UAE region, a daily precipitation data at a horizontal resolution of 10km (0.1^0 grid) is selected. It is true that the satellite-based precipitation measurements have a bias from the ground measured data [28]. Moreover, it is clear that an accurate and timely monitoring of precipitation still remains a challenge in this hyper-arid region. As such, and to enhance the quality of the precipitation, fusion of the satellite driven precipitation, radar and rain gauges is crucial [6]. Taking the bias into account, Mahmoud et al [32], showed that the rainfall distribution patterns across the UAE, especially in the northeastern part and mountainous area, obtained from the ground measurements (rain gauges), had a high correlation (with RMSE less than 15mm) with the GPM's final run precipitation products. Evidence from Wehbe et al study [6] also revealed that the GPM product captures most events in the North eastern highlands but with constant underestimations compared to the gauge records. Therefore, the dataset of GPM-IMERG final run precipitation was adopted as it can provide a continuous record of the rainfall variability over the UAE. This will serve as a reliable product to complement ground precipitation measurements for ungauged or poorly gauged areas. This final estimate of the daily accumulated precipitation dataset is derived from the half-hourly record. The dataset is produced at the NASA Goddard Earth Sciences (GES) Data and Information Services Center (DISC) after adding the valid precipitation retrievals for the day. Since GPM can cover areas

where there are no ground based measuring stations, this makes GPM precipitation data as the best source of input for hydrological modelling.

3.3.1. Water body detection

The optical sensors' spatial resolution is mostly categorized into three groups as high resolution sensors (<5 m), medium sensors (5–200 m), and coarse sensors (>200 m), according to [67].

1. High-spatial resolution sensors

These sensors are known for their higher level of accuracy. Day to day, research in remote sensing is performed so that sensors capable of achieving a higher spatial resolution can be developed. As a result, significant advances were made so far. Some of the newly developed sensors, already on board, are IKONOS, Rapid Eye, Worldview, ZY-3, Quick bird, and GF-1/2. These are capable of providing images with spatial resolutions ranging from a few centimeters to meters. At this level of resolution, and despite their limitations of reduced spatial coverage, small water bodies and even paths of small streams can be successfully detected. The data of the sensors are not freely available, meaning that they are not extensively used.

2. Medium-spatial resolution sensors

These sensors are known for their medium level of accuracy. The commonly used sensor in this category is Landsat. Landsat is known as one of the most successful satellite series in history. During the early mission of Landsat, Multispectral Scanner (MSS) were used but later on it was upgraded, in Landsat-4 and Landsat-5, to Thematic Mapper (TM). On landsat-7 the sensors used were Enhanced Thematic Mapper Plus (ETM+). The latest sensors known as Operational Land Imager (OLI) and Thermal infrared sensors (TIRS) are used in the Landsat-8. The range of the sensors, spatial and temporal resolution, number of available bands are shown in *Table 3-1*. Resolution at a level of 30m is ideal for detecting surface water bodies. In this thesis, Landsat-8 was adopted for the detection and extraction of the water in the reservoir because of its higher spatial resolution, versatility and free availability [68], [69], [70], [71], [72], and [73].

3. Coarse-spatial resolution sensors

These sensors are known for their low level of accuracy since they cover large areas with more information at a bigger scale but possess high resolution at the temporal scale with wide coverage. For instance, the Advanced Very High Resolution Radiometer on board National Oceanic and Atmospheric Administration satellites (NOAA/AVHRR) was originally planned to monitor the

ocean and atmosphere, but later on, as per the reports of [74], it detected effectively large-scale flood events. Another sensor is the MODIS, which falls in this category. Since 2000, data from MODIS has been applied in many fields such as atmospheric monitoring, land cover or land use changes and has also been used in the detection of surface water [75], [76]. Another sensor launched in 2011 is the Visible Infrared Imaging Radiometer Suite onboard Suomi National Polar-orbiting Partnership (Suomi NPP-VIIRS). This sensor has a higher spectral resolution ranging spatially from 375m to 750m, and has the capacity to detect surface water according to [77]. MEdium Resolution Imaging Spectrometer (MERIS), developed by the European Space Agency (ESA), collected 300m spatial resolution multispectral information (used for water surface detection) from 2002 to 2012 [78].

Types	Sensor/Satellite	Number of Bands	Temporal Resolution (day)	Spatial Resolution (m)	Maximum swath at nadir (km)	Scale of Application[a]	Availablity (freely)	Data Availability
High Resolution	IKONOS	5	1.5-3	1-4	11.3	L-R	NO	1999--
	QuickBird	5	2.7	0.61-2.24	16.5	L	NO	2001--
	WorldView	4-17	1-4	0.31-2.40	17.6	L	NO	2007--
	RapidEye	5	1-5.5	5	77	L-R	NO	2008--
	ZY-3	4	5	2.1-5.8	50	L-R	NO	2012--
	GF-1/GF-2	5	4-5	1-16	800	L-R	NO	2013--
Medium resolution	Landsat	4-9	16	15-80	185	L-G	YES	1972--
	SPOT	4-5	26	2.5-20	120	L-R	NO	1986--
	Aster	14	16	15-90	60	L-G	YES	1999--
	Sentinel-2 MSI	13	5	10-60.	290	L-R	YES	2015--
Coarse Resolution	NOAA/AVHRR	5	0.5	1100	2800	R-G	YES	1978--
	MODIS	36	0.5	250-1000	2330	R-G	YES	1999--
	Suomi NPP-VIIRS	22	0.5	375-750	3040	R-G	YES	2012--
	MERIS	15	3	300	1150	R-G	YES	2002-2012
	Sentinel-3 OLCI	21	2	300	1270	R-G	YES	2016--

Table 3-1*:* Space borne Sensors Commonly used for Surface Water Detection adapted from [67].
[a:] L: landscape; R: regional; G: global; L-R: landscape to regional; L-G: landscape to global; R-G: regional to global.

The extraction of the surface area of a water body, such as lakes and reservoirs is important for the surface water resource management and environmental monitoring. This extraction can either be performed by the traditional field survey method, which requires visiting of the area, or by relying on satellite for acquiring remotely sensed images. There are many limitations for the former, such as the spatial coverage and temporal resolution [79]. However, the latter has a large observation range, very high speed, high accuracy, Ironic and precise measured information, as well as low costs, as most of the data is freely available in the web [80]. From the numerous satellites used in obtaining remote-sensed images of the surface area of a water body, the Landsat satellite was chosen since its imagery is one of the most widely used data in extracting surface water information, owing to its sensitive response to surface water and also spectral resolution [81].

The Landsat-8 satellite consist of two sensors, OLI and TIRS, providing seasonal coverage of the globe at a horizontal resolution of 15m for panchromatic (band 8), 30m for the visible, NIR and SWIR bands and 100m for the thermal infrared. These bands are used for calculating indices such as normalized difference vegetation index (NDVI), normalized difference water index (NDWI), and modified normalized difference water index (MNDWI) and so on. The detail calculations for determining the indices and their use is discussed in sections 3.5.4 and 3.5.5. Landsat 8 was developed by NASA and USGS and launched to space on February 11, 2013. Since then it has provided images that are useful for land use planning and monitoring of water bodies on regional and local scales [82]. Images of the reservoir for different events captured by Landsat-8 OLI were used during the calibration and determining the efficiency of the hydrologic model. Discharge data is required for model calibration and verification. However, there was no recorded stream flow by any gauging station throughout the stream (wadi) network. From previous studies on this area, there used to be one gauging station in Bitha but it was destroyed in the early 1990 after a heavy flooding event in the basin. To the best of the author knowledge, from that time onwards, the wadi flow has never been measured. Given this, the author has to come up with an alternative solution for the calibration of the model and to assess its performance. Since the entire work is dependent on remote-sensed data, the author preferred to obtain the volume of water stored in the dam (Fujairah/Ham dam) from satellite images. *Figure 3-3(a)* shows the bird eye view of the reservoir. *Figure 3-3(b-e)* show classified surface areas (after being supervised) of the water body at march 24, 2014, March 13, 2016, March 03, 2018 and March 29, 2019 respectively. As a matter of fact, this approach/method can also be used in calculating the volume of inaccessible water bodies and estimate the volume of the water body directly. This approach was used for detecting and extracting water surface and its variation (change) with time by Guo et al. [81] in Tianjing, China ; Rokni et al.[83] in lake Urmia, Iran; Ghebreyesus et al. [84] in Al-Ain, UAE; Lu et al.[85] in Xiong'an, China; Du et al.[86] in Qingjiang river basin, China; Tang et al.[87] in Yangtze river, China, and El-Asmar et al.[88] in Nile valley delta, Egypt. Likewise, in this study this approach was used to calibrate the model. The volume of the reservoir was estimated by multiplying the extracted surface area of the supervised water body images captured by satellite during the aforementioned events, with the depth of the reservoir derived from the DEM. Once the volume was calculated, a comparative analysis was performed with the estimated (simulated) volume at the outlet section (Fujairah/Ham dam). The observed (calculated) volume is the volume calculated from the images captured by Landsat-8 satellite (OLI) during the rainfall events.

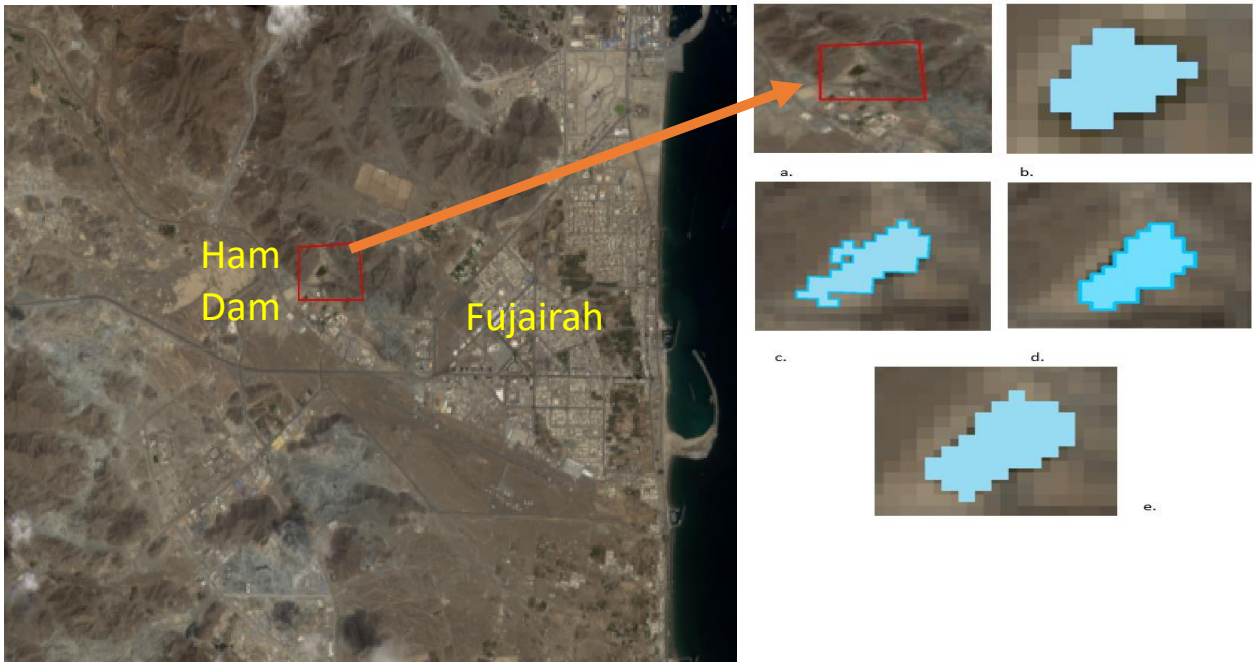

Figure 3-3*:* (a) Areal view of the Ham reservoir (the dark color inside the red box); Supervised and classified Landsat Images of Ham reservoir on (b) March 24,2014; (c) March 13, 2016; (d) March 03, 2018 and (e) March 29, 2019

3.4. Modelling with HEC-HMS

The Hydrologic Modelling System is designed to simulate the rainfall-runoff processes in dendritic watershed systems. This model has its own capabilities and limitations. It has been used worldwide and preferred over other simulation software for the following reasons;

- Capability to represent the watershed characteristics,
- Meteorology description,
- Hydrologic simulation,
- Parameter estimation,
- Forecasting flows,
- Evaluating depth area effects,
- Sediment flows and
- Capability to be connected with GIS.

The advantage of using the geographic information system (GIS) in hydrological management was stated by many researchers [89], [90], and [91]. However, due to the choice made in the design and development of the software, the limitations are confined to two aspects: model formulation and flow representation. Since all the mathematical models are deterministic and not stochastic, all the boundary conditions are known from the beginning and are somehow stationary in time. During

long periods of time (for continuous-based simulations), it considers the initial state of the boundary but does not consider the change in the boundary condition, which can be caused by humans or other processes for the simulation period considered. The second limitation is in the design of the basin model for the dendritic network. This kind of design only allows the hydrologic element to have one downstream connection, which prevents the outflow to split into a different element. In practical terms, this means the branching or loop stream network is not possible and the design does not allow or consider any simulation for the back water in the stream network.

For regions with arid environment like the UAE, priority should be given to the research for improved hydrological models with better methods for precipitation observation and modeling. According to [92], [93], [94], [95], and [96], modelling with a simple methodology and a few parameters is considered to be the best approach in the runoff modelling. With this in mind, only few parameters were used in this study. Let us discuss about the three main components in HEC-HMS: basin model, precipitation model, and control specifications.

3.4.1. Basin Model

The basin model is the main component of the project as it is used for converting the atmospheric conditions (precipitation) into stream flows within the watershed. In this model, the schematic flow diagram and manipulation of the values was performed. For each sub basin, the geographic coordinates, area, loss of water through canopy and surface methods were determined. The transformation of the rainfall excess to runoff and base flow methods were also the major functions performed. A gridded model, which is also called as cell-based model, was adopted in this study. This includes the coordinate system and cell size. *Figure 3-4* shows the wadi Ham's 5 sub basins used in the rainfall- Runoff modelling.

Each sub basin shown in *Figure 3-4* represents the physical areas within the basin and produce a runoff hydrograph at the outlet of their respective sub basins. The produced hydrograph is the net difference of the precipitation (rainfall) data and the loss of surface water. According to [97], the final excess precipitation (rainfall minus loss) is transformed into runoff at the outlet using empirical methods such as the conceptual or the kinetic wave. In this model, the loss rate is simulated by the deficit and constant method. This method uses a single soil layer to account for continuous changes in moisture content and calculates the loss by combination of the canopy method in response to the evapotranspiration computed in the meteorological component of the model.

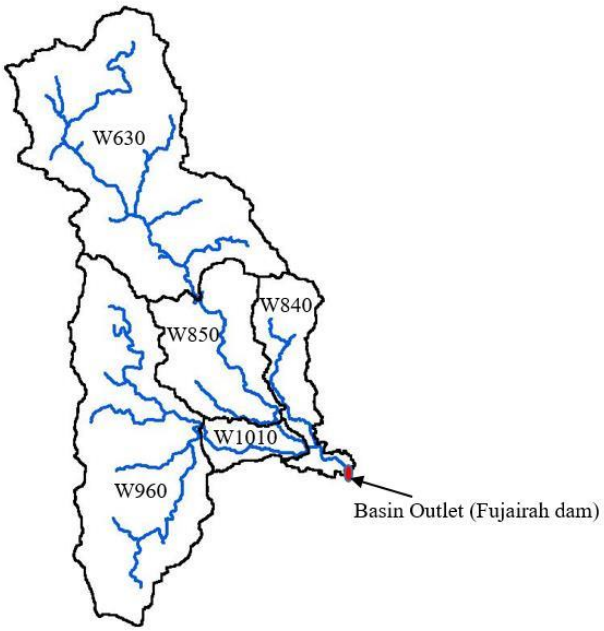

Figure 3-4: Wadi ham sub basins used in the rainfall- Runoff modelling

The deficit and constant method is used along with the canopy method to extract water from the soil in response to potential evapotranspiration calculated in the meteorological model. The initial deficit is the initial condition where water is required to fill the soil layer (only the upper layer) for maximum storage. This value could be initialized with zero. The maximum deficit is the second parameter in this loss method adopted. This parameter shows the maximum water the soil layer can hold. The third parameter is the constant rate defined as the percolation rate when the soil layer is saturated. Initially this value could be approximated to the saturated hydraulic conductivity of the soil. The last parameter is the imperviousness of the soil. The higher the impervious area the lesser the loss value will be and the more runoff generated.

From the different methods or techniques set by Hydrologic Modeling Center, for the transformation of rainfall excess into surface runoff, the Mod Clark method is adopted since the precipitation is gridded data. This method is a linear, quasi-distributed transform method trying to represent the sub basin as a collection of grid cells. This method uses the index for each cell's travel time, time taken by the water to move from one cell to another, scaled by the total time of concentration.

HEC-HMS has methods such as bounded recession, constant monthly and linear reservoir and non-linear Boussinesq for base flow calculations. Base flow considers the normal flow through a channel

or the effects of it on groundwater. For this study, and due to the absence of reliable data for initializing the parameters, the base flow was not considered.

A reach is an element with one or more inflow and only one outflow. In HEC-HMS a reach is used to model a river, stream or wadi. Flood routing through HEC-HMS enables us to use either of the following methods: simple lag, Modified-Plus, Muskingum, Muskingum-Cunge, kinematic wave and Staddler Stagger methods. Since Muskingum method implements the conservation of mass concept to route the flow, it was adopted in this wadi. Initially, an acceptable approximate values of the storage coefficient (k) and the weighting factor (x) for the effect of the inflow and outflow of the storage were set. Later on, the reach flow was calibrated to determine the exact values of k and x for this wadi.

Nineteen hydrologic elements were selected in the simulation model of wadi Ham made up of five sub basins, seven reaches, and seven junctions as shown in *Figure 3-5*. Geometric data, including area of each sub basin and length of reaches, are shown in *Table 3-2*.

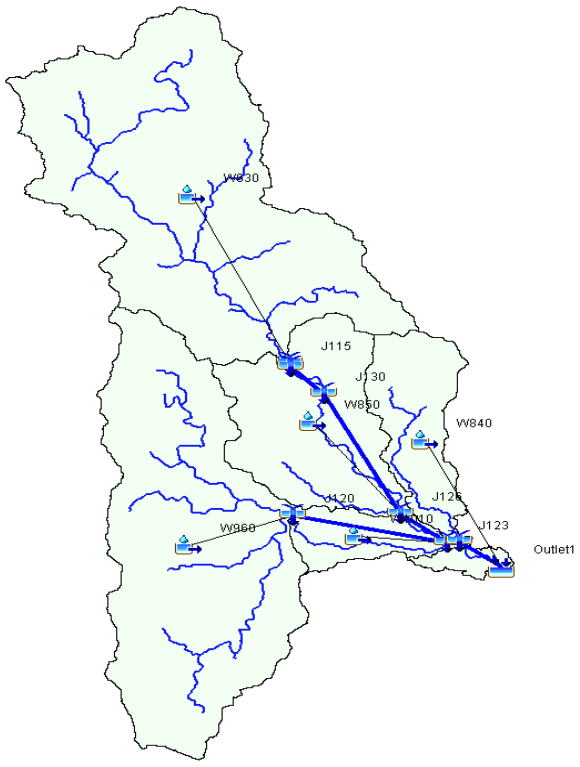

Figure 3-5: Basin model setup for the Wadi Ham in HEC-HMS (W=sub-basin element, J=junction element)

3.4.2. Precipitation Model

The meteorological component of this model is in charge of preparing the boundary conditions that act on the watershed during simulation. For basins with sub basin elements, the meteorological

model needs to specify how the precipitation value will be generated for each element. For this study, since the simulation is set for a minimum of two months, it is considered to be a continuous simulation. For such conditions, the evapotranspiration (ET) should be taken into account in order to prevent unrealistic runoff. ET is a mode of returning water to the atmosphere from the ground surface by evaporation, and from vegetation cover by transpiration. Therefore, the Hamon method was adopted for calculating the loss of water due to ET in this model under the Deficit and Constant loss method. Hamon [46], clearly stated in equation (1) that this method is purely an empirical relationship between saturated water vapor concentration and potential evapotranspiration at the mean daily air temperature.

$$PET = 29.8\mathrm{D}\frac{e_s^*(T_a)}{T_a+273.2} \qquad (1)$$

$$e_s^*(T_a) = (2.7489 \text{ x } 10^8)\, exp\left(\frac{-4286}{(T_a+242.79)}\right) \qquad (2)$$

The daily estimate of evapotranspiration is in mm, D is the possible duration of sunshine in units of 12 hours (daylight time); air temperature (T_a) in degrees Celsius (^oC) and saturated vapor pressure (e_s) is a function of air temperature.

The meteorological model of HEC-HMS requires either the historical time series of precipitation data from ground based stations or gridded precipitation from satellites. The gridded precipitation is used to simulate only runoff in a gridded basin. The gridded precipitation data of several storm events in 2014 (Feb –Apr), 2016 (Mar –May), 2018 (Jan –Mar) and 2019 (Jan –Apr) written in HEC-DSS was imported in HEC-HMS through the grid data manager. The maximum return period for the rainfall events considered is 8 years.

		Drainage Area (km^2)			**Drainage Length (m)**
Sub basin	W630	77.19	**Reach**	R280	126.2
	W840	16.87		R290	1,407.5
	W960	64.69		R400	4,863.2
	W1010	7.42		R440	1,727.0
	W850	26.78		R450	372.5
				R460	4,726.3
	Total	193.0		R480	1,733.5
				Total	14,956.3

Table 3-2*:* Geometric data of the basin ("W" and "R" followed by numbers are the names of the sub basin and reach elements when used in HEC-HMS)

3.4.3. Control Specification

The control specifications is the main component of the project. It provides the simulation specific information for each event such as start and end date and time and, most importantly, the simulation time. All the control specifications were set based on the length and depth of the events selected in the study area.

3.5. Methodology

The proposed method is composed of five phases:

a. Acquisition of precipitation,
b. Watershed delineation from the DEM,
c. Use of gridded GPM precipitation dataset in HEC-HMS,
d. Obtaining satellite images of the water body using Landsat-8 and,
e. Mapping surface water body for calibration of the simulated volume of the water body.

3.5.1. Precipitation data

i. Gridded precipitation is downloaded from the NASA website (https://pmm.nasa.gov/data-access/downloads/gpm)
ii. Processing the bulk data in MATLAB (cleaning, converting it from netcdf to raster file and importing it in ArcMap).
iii. Re-projecting, masking and converting the format from raster to ascii
iv. Through a batch file, the bulk precipitation data from step (iii) was written and stored in HEC-DSS, making it ready to be imported in HEC-HMS.

3.5.2. Watershed delineation

Using the DEM of the study area, the delineation of the watershed and generation of stream flow was performed with HEC-GEOHMS in ArcGIS. It was carried out based on the delineation procedure available in Arc-Hydro and HEC-GEOHMS extensions. The watershed modelling system inbuilt in this extension was then used for extracting the basin characteristics such as sub basin features (area, slope, centroid and elevation) and river characteristics (length, slope and centroid). These physical characteristics of the sub-basins and streams were used to estimate the hydrologic parameters of the basin model. By specifying a control point at the downstream outlet section (location of the dam), the downstream boundary for the HEC-HMS project was defined. Moreover, the precipitation grid was also overlaid on the watershed, and in this grid the cells are assigned to the sub basins of the model. It is very important to note that the coordinate system and

the cell sizes selected are the same as those used in geo-referencing the precipitation data. Finally, the gridded sub basin and stream paths, derived from the water shed modelling system inbuilt within the HEC-GEOHMS, were imported to the main component, basin model, of HEC-HMS.

3.5.3. GPM Precipitation as HEC-HMS input

After setting the gridded basin model, the gridded GPM precipitation estimates were the main inputs to the HEC-HMS model. A script in MATLAB was written to clean and process the raw precipitation dataset retrieved from GPM-IMERG database system. After providing the specific folder for each dataset, each precipitation file was again reprocessed in ArcMap through the model builder function for projection, conversion and masking as per the specification of the gridded basin. GPM data is particularly useful as an input to models of such watersheds that do not have dense ground precipitation gauge networks. As such, the information about the spatial distribution within the watersheds improved the estimate of the basin averaged precipitation.

3.5.4. Landsat-8

For the comparative analysis of the simulated volume and the observed volume of water in the reservoir (Fujairah/Ham dam), only four images of Landsat-8 OLI data attained on 24 March 2014, 13 March 2016, 03 March 2018 and 29 March 2019 obtained from the USGS Earth visualization viewer, were used. All these images were selected based on the historical records of heavy storm events in the study area. Entire images were pre-georeferenced to UTM zone 40N projection using WGS-84 datum. According to Schroeder [98] and documentation in Landsat 8 [99], the spectral radiance data is converted to planetary reflectance using the reflectance rescaling coefficient provided in the meta data file using equation (3) and (4) as shown below. Landsat 8 [99], and Chavez [100] developed a method for converting calculated satellite reflectance using equation (3) to fully corrected surface reflectance with local sun elevation as in equation (4). Once the radiometric calibration and atmospheric correction was performed after being re-projected and mosaicked, the images were ready for classification and the values can then be used for calculating the water indices.

$$\rho_{\lambda'} = M_\rho . \theta_{cal} + A_\rho \qquad (3)$$

$$\rho_\lambda = \frac{\rho_{\lambda'}}{cos\theta sz} = \frac{\rho_{\lambda'}}{sin\theta se} \qquad (4)$$

$$\theta sz = 90 - \theta se \qquad (5)$$

$\rho_{\lambda'}$ is the Top of Atmosphere planetary reflectance, M_ρ is multiplicative rescaling factor, A_ρ is additive rescaling factor, θ_{cal} is quantized or calibrated standard product pixel value (band), ρ_λ

is corrected planetary reflectance (solar angle correction included), θsz is the local solar zenith angle, and θse is local sun elevation angle.

3.5.5. Mapping of Surface water of reservoir

In today's world, the use of remote-sensed multi-spectral images for mapping or extracting the surface's water body is one of the main methods adopted. The underlying principle is the difference of absorption and reflection of light between water and other features such as sand, gravel or vegetation in different frequency bands. In studies performed by [101] and [102], the balance between rainfall and evaporation and interactions between surface and ground water systems is shown by the volume of water in lakes, and reservoirs. Based upon the availability of morphological data, the volume of water bodies at any particular event can be calculated with numerous methods. For regions like the UAE with no existing gauging instruments, relying on remotely mapped water body is the only viable option. For instance, Dawit et al. [84] used the Landsat images to determine the extent of agricultural and green areas in Al Ain, UAE. The images of Landsat-8 OLI with the same spatial resolution at different events are first processed and the surface area of the water body subsequently based on their pixel values. Only the remote-sensed images during events of high rainfall and cloud free days were adopted in this study. Two methods have been implemented, which resulted in the same surface area of the water body.

First method

Calculate the surface area of the water body using the NDWI and MNDWI indices. This is performed in equations (6) and (7) using three bands namely green, near-infrared (NIR) and short-wave infrared (SWIR) wavelengths. This is justified by the fact that the water reflections are less pronounced in the infrared compared to the visible wavelength. McFeeters [103] developed a method for determining NDWI, equation (6), to delineate open water bodies with visible green light and reflective radiation. This method was updated by Xu [104] to modified normalized difference water index (MNDWI), as per equation (7), by using short-wave infrared radiation instead of near-infrared rays. This classification was done based on the pixel color difference. The color of the pixel with positive values in both NDWI and MNDWI represents the water body after it has been cross checked with the actual water body seen in Google Maps. This finding is consistent with the remarks made by both [103] and [104]. A representative map of the water body indices for the water reservoir in 24 March 2014 is shown in *Figure 3-6* where the water body is shown by the blue color.

$$NDWI = \frac{Green-NIR}{Green+NIR} \qquad (6) \qquad MNDWI = \frac{Green-SWIR}{Green+SWIR} \qquad (7)$$

Once the surface area of the water body is mapped, the volume of the water stored in the reservoir is calculated after extracting the depth of the reservoir from DEM.

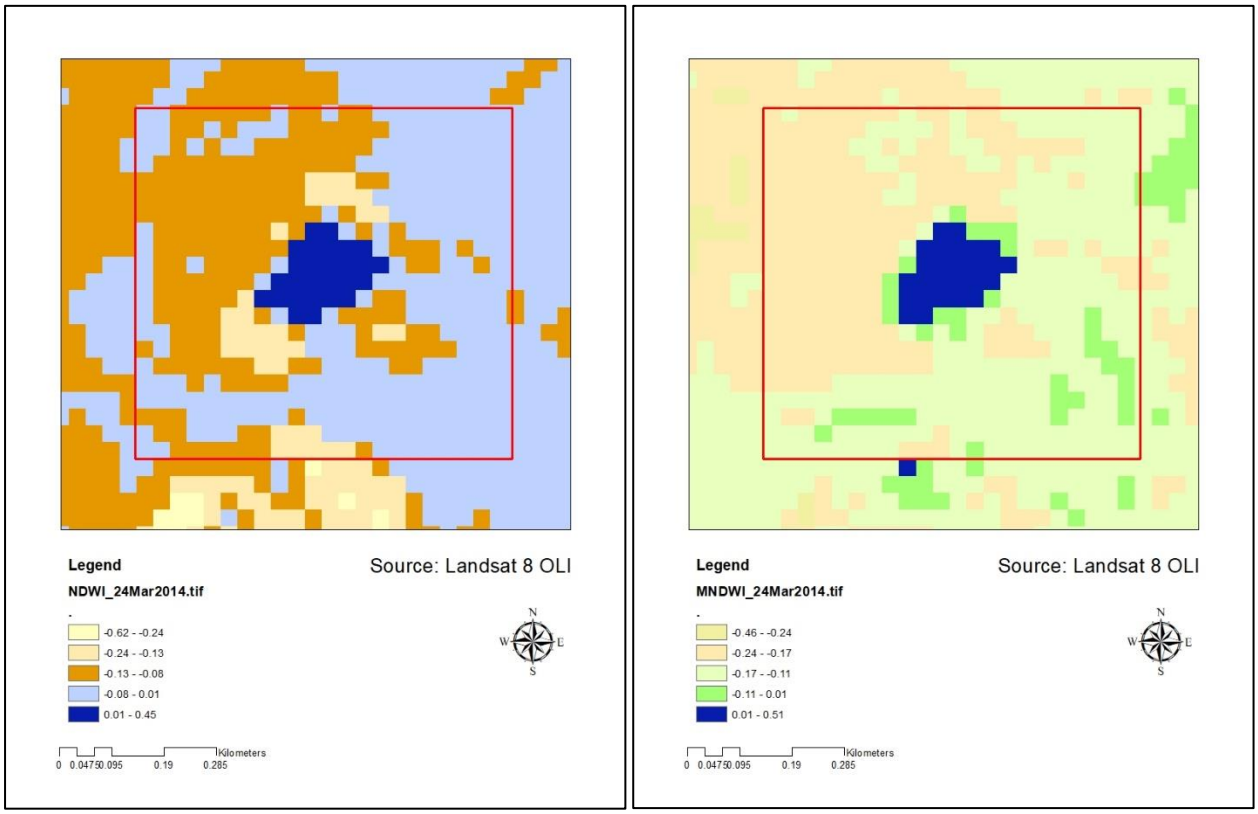

a. b.

Figure 3-6: (a) NDWI image of the Ham reservoir; (b) MNDWI image of the Ham reservoir; the blue color is the water body in both figures. The red Box used is for targeting the water body.

Second method

The surface area of the water body was computed directly from the remote-sensed image after it had been composited, clustered, and classified as per its features. The composition is done only for the visible wavelength. After classifying the features, using the iso-clustering technique, the shape of the water body was visually identified by comparing it with the actual size and location when seen from Google Maps. This raster water body was later converted to a vector to make it easy in calculating the surface area of the water body. Finally, using the mapped surface water body and extracting the depth of the reservoir from DEM, volume of the stored water in the reservoir was calculated as shown in *Table 3-3*. The generated maps were overlaid to produce the reservoir surface area maps at different events from 2014 to 2019 as shown in the previous page *Figure 3-3*.

Year	Surface area (m^2)	Volume (x 10^6 m^3)
March 24, 2014	45,091.0	0.23637074
March 13, 2016	48,900.0	0.22301606
March 03, 2018	41,093.9	0.14625785
March 29, 2019	53,800.0	0.32637074

Table 3-3*: The surface area and volume of the reservoir calculated from Landsat images in the specific dates*

3.6. HEC-HMS Simulations

After defining the control specifications, a unique simulation model was set up for each rainfall event. According to the highest storm events in the past seven years, it is being recorded that most of the heavy rain events occur in the month of March. From the selected years, 2014, 2016, 2018 and 2019 simulated runoff or stream flow had been obtained in HEC-HMS after the boundary conditions were specified for each event separately. According to the reports found in the soil map [56], and the geological maps reports by British Geological Survey (BGS) in 2006 [51], the soil is mostly sand and gravel with alluvial deposits at the lowlands. Hence, the hydraulic conductivity of sandy loam soil to sandy soil ranges from 6 to 21cm/hour according to Rawls et al. [105]. *Table 3-4* show the maximum storage volume of the runoff in million cubic meters for each sub basin and the cumulative discharge at the outlet section (Ham dam). From the geological study of the area [56], the area covered by the sandy soil and alluvial deposits was roughly calculated by hand. After deducting this value from the total area of the basin, the impervious area came up to be 10% of the Ham basin. Using this value, the hydrological model was initiated for simulation. The simulated volume of runoff collected at the outlet section (Ham dam) was found to be much higher than observed one in all the events. For the efficacy of the hydrological model and its subsequent use, the exact covered area by impervious soil should be clearly identified. Hence, calibration of the hydrological model was performed by reducing the percentage of impervious area from 10% one by one and comparing the simulated volume with the observed one as shown in *Table 3-5*. Considering the mean absolute mean difference value after the calibration, it was found that the maximum area of the impervious soil was only 2% of the total basin's area, which is equivalent to 4km^2. This value was used for the calibration of the simulated volume with the observed stored volume in the reservoir. *Table 3-5* shows how sensitive the model was to a change in the area of the impervious soil. The table also showed the difference in volume between the observed and the simulated volume of water stored in the dam by the runoff generated from the precipitation.

	Feb – Apr 2014	Mar – May 2016	Jan – Mar 2018	Jan – Apr 2019
Hydrologic Element	**Volume ($10^3 m^3$)**	**Volume ($10^3 m^3$)**	**Volume ($10^3 m^3$)**	**Volume ($10^3 m^3$)**
W630	47.7	177.6	47.7	177.6
W840	10.2	32.2	10.2	32.2
W960	37	120.9	37	120.9
W1010	4.4	14	4.4	14
W850	16.1	51.5	16.1	51.5
Outlet (Ham dam)	**115.4**	**396.2**	**115.4**	**396.2**

Table 3-4: Global summary of the simulated stored volume of runoff for each sub basin

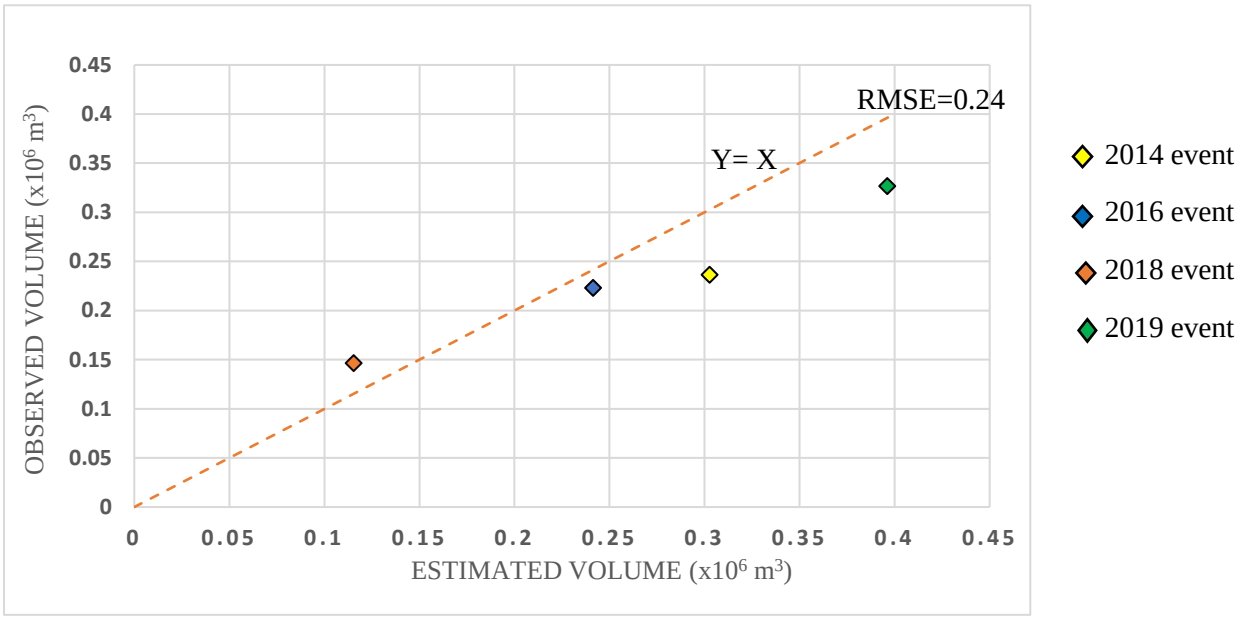

Figure 3-7*:* Comparison between Observed and Simulated Storage in Ham (Fujairah) Dam

Volume, 2014		Estimated (10^3m^3)	Observed (10^3m^3)	Difference	%
Impervious Area	**2%**	302.7	236.37074	66.33	28.06
	3%	461.5	236.37074	225.13	
	5%	769.6	236.37074	533.23	
	10%	1513.7	236.37074	1277.33	
Volume, 2016					
Impervious Area	**2%**	241.4	223.01606	18.38	8.24
	3%	362.2	223.01606	139.18	
	5%	603.6	223.01606	380.58	
	10%	1207.2	223.01606	984.18	
Volume, 2018					
Impervious Area	**2%**	115.4	146.25785	30.86	21.10
	3%	173.1	146.25785	26.84	
	5%	288.5	146.25785	142.24	
	10%	576.9	146.25785	430.64	
Volume, 2019					
Impervious Area	**2%**	396.2	326.37074	69.83	21.40
	3%	594.2	326.37074	267.83	
	5%	990.4	326.37074	664.03	
	10%	1980.8	326.37074	1654.43	

Table 3-5*:* Calibration of the modelled volume of the runoff by changing the area of impervious soil

The simulated and observed water storage values for this wadi during the four events considered after calibration are as shown in *Figure 3-7*. From *Table 3-5*, it can be clearly seen that with the 2% of the total area of the basin being impervious, the absolute relative error in percentage was found to be optimal (or accepted) when compared to a similar study performed by sheriff et al. [55]. For the 2014, 2018 and 2019 events, the errors were the highest but this was only due to the different time stamps used for estimated and observed volumes. The simulated stored water was the result of the runoff cumulated for the precipitation event from February to the end of April, 2014. However, the observed volume of the reservoir was considered from the status of the reservoir on March 24, 2014. Hence, the simulated volume gave a higher value by 66 $x10^3$ m^3 which is equivalent to 28% higher than the observed volume. This extra volume is due to the runoff flow after March 24, 2014. These different values are expected since there will be additional flow of water to the reservoir for the events after March 24 as shown in *Figure 3-8 (a)*. The time series plots of the streamflow/ runoff at the outlet section for each event are illustrated separately *Figure 3-8 (a-d)*. This additional flow of water/runoff made the simulated/estimated volume to increase. Likewise, the same reason applies for the differences in volume stored for both the estimated and

the observed one during the 2018 and 2019 events. However, for the Mar-May 2016 event the error was only 8% equivalent to 18 $x10^3$ m^3 even though the time stamp for both the simulated volume and observed volume are different. This was because there was only higher rainfall in the first two weeks of March, 2016 which is able to create runoff. After that the precipitation recorded was too low to create more runoff to reach the outlet section. Hence, the final calibrated simulated runoff hydrographs and stored volume at the outlet were considered to be optimal values and proceeded for the next phase, which consists on the simulation of the hydraulic models and generation of flood depth and velocity maps within the flooded zone of the basin.

a.

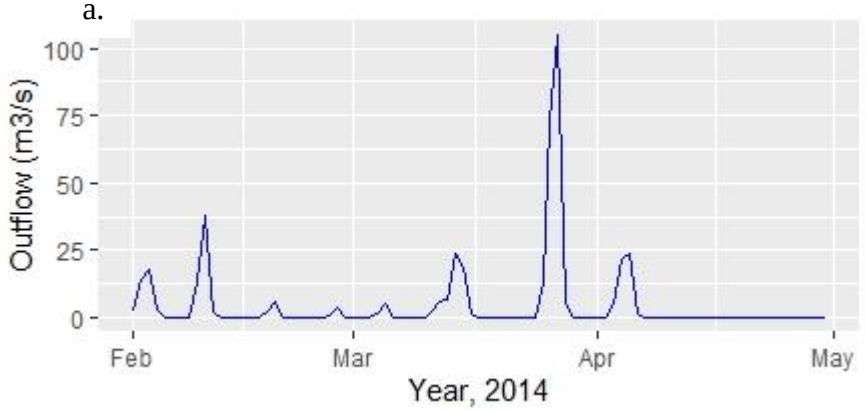

b.

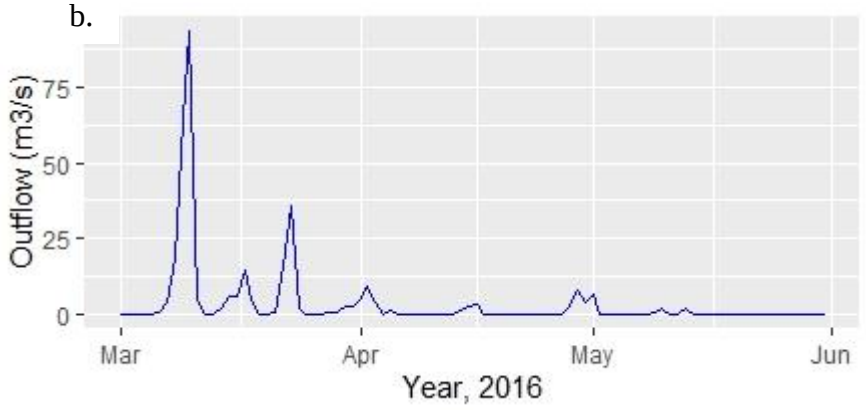

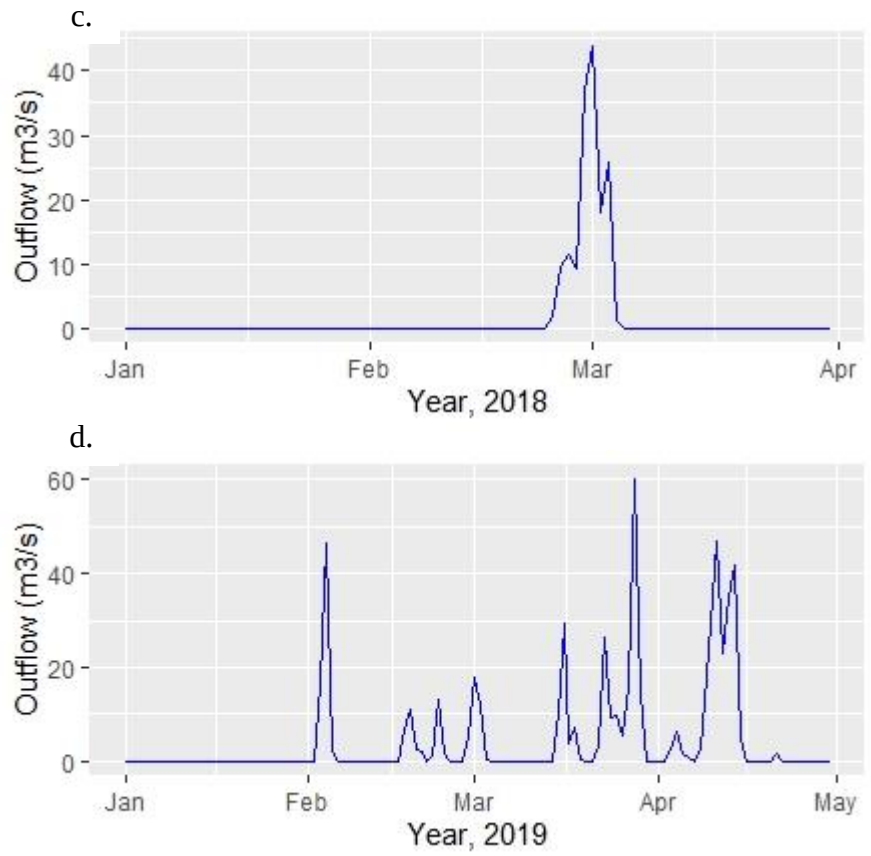

Figure 3-8 (a-d): Time series of the calibrated stream flow at the outlet section (Ham dam) during several events

Figure 3-9 to *Figure 3-13* give the daily time series of rainfall and the equivalent calibrated runoff in each sub basin and for different events. They clearly show the relationship between the magnitude of the rainfall and the runoff generated for the specific study area. The final output of the simulated runoff hydrograph was achieved after being calibrated with the change in imperviousness of the land. A value of 2% for the imperviousness factor was adopted since the estimated volume in the reservoir varied from the observed one by a small amount as shown in *Table 3-5*. From the basics of hydrology, for surface runoff to occur as flash flooding, the rainfall intensity should exceed the evaporation rate and infiltration capacity of the soil. Bearing this in mind, the type and texture of a soil are vital factors in determining the infiltration and water holding capacity of the area and consequently the flood vulnerability [106]. Even though the area is considered as a dry area, rapid runoff is common even in the case where the magnitude of the precipitation is low. This is mainly due to the intense but short duration of the rainfall, soil type and slope of the area. As a general rule, runoff from intense rainfall in clay soils is likely to be more rapid and greater than in sand as there is more infiltration in sandy soils. The second variable which affects the runoff magnitude and velocity is the surface slope. This is one of the major elements in the runoff volume. The wadi Ham's main tributary originates from the sub basin W630, which

covers more than 77km^2 in area originating from highlands of Massafi town. The steep channel of the wadi in this area makes it to flow with higher speed and larger volume as shown in *Figure 3-9*. On the other hand, for a similar amount of rainfall (2014-2019) on the other sub basins, such as sub basin W1010 with area of only 7.42km^2 located on the flat plains of the Fujairah, there is hardly any runoff as most of the rainfall in the area infiltrates into the soil as shown in the daily time series of the rainfall vs outflow (runoff) within the sub basin in *Figure 3-13*.

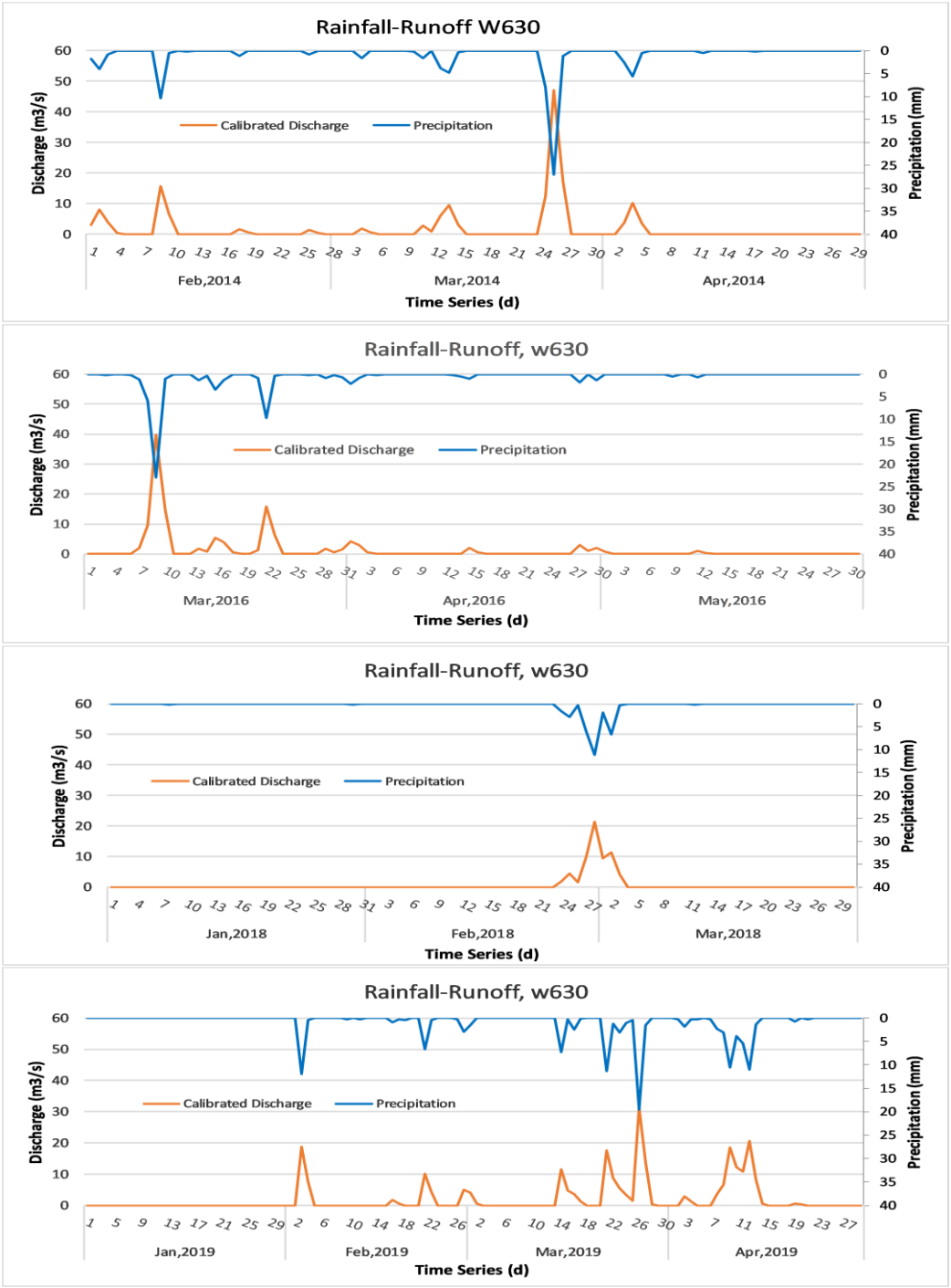

Figure 3-9*:* Precipitation, calibrated Discharge from Sub Basin-W630 at different events

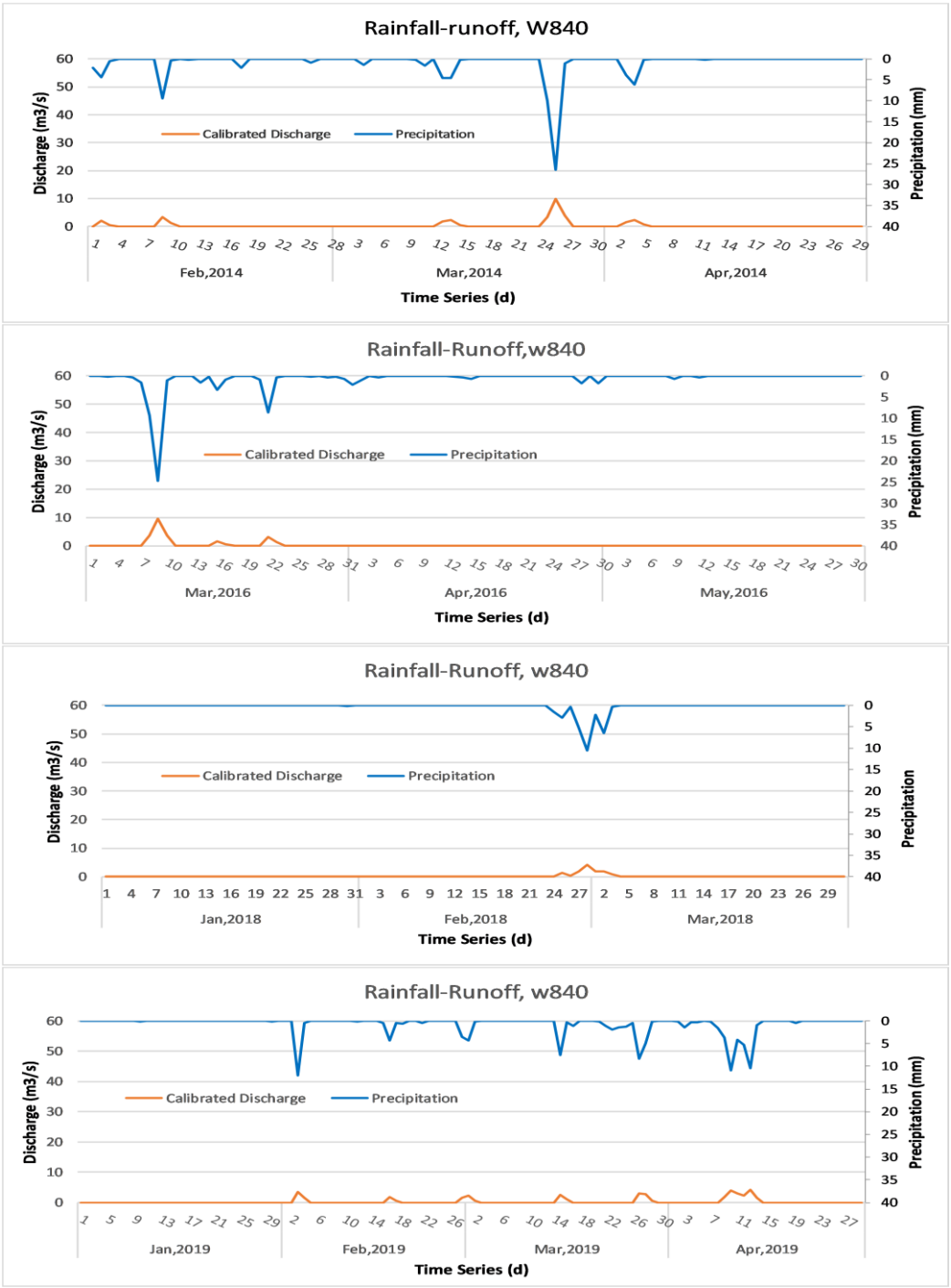

Figure 3-10*:* Precipitation, calibrated Discharge from Sub Basin-W840 at different events

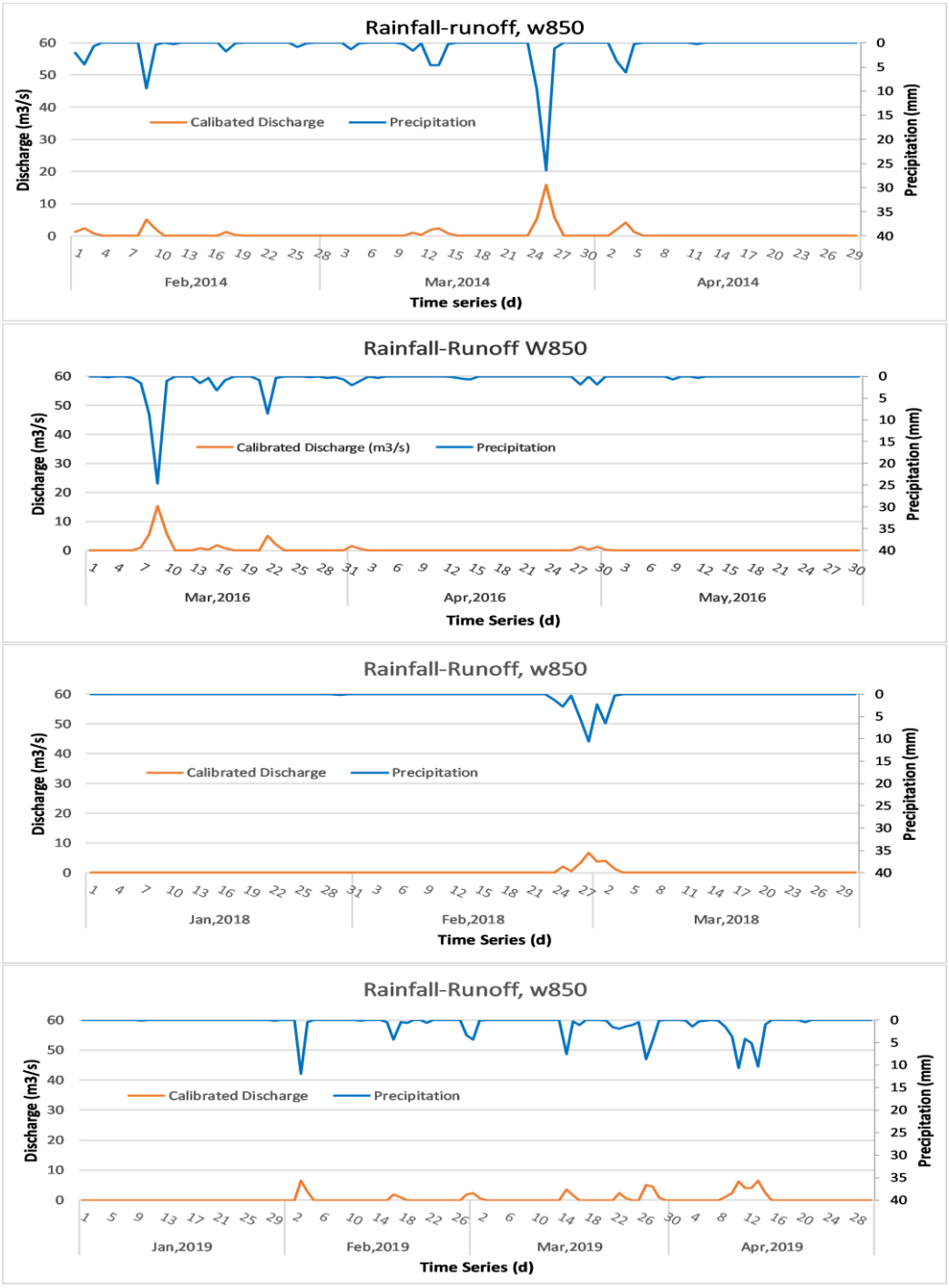

Figure 3-11*:* Precipitation, calibrated Discharge from Sub Basin-W850 at different events

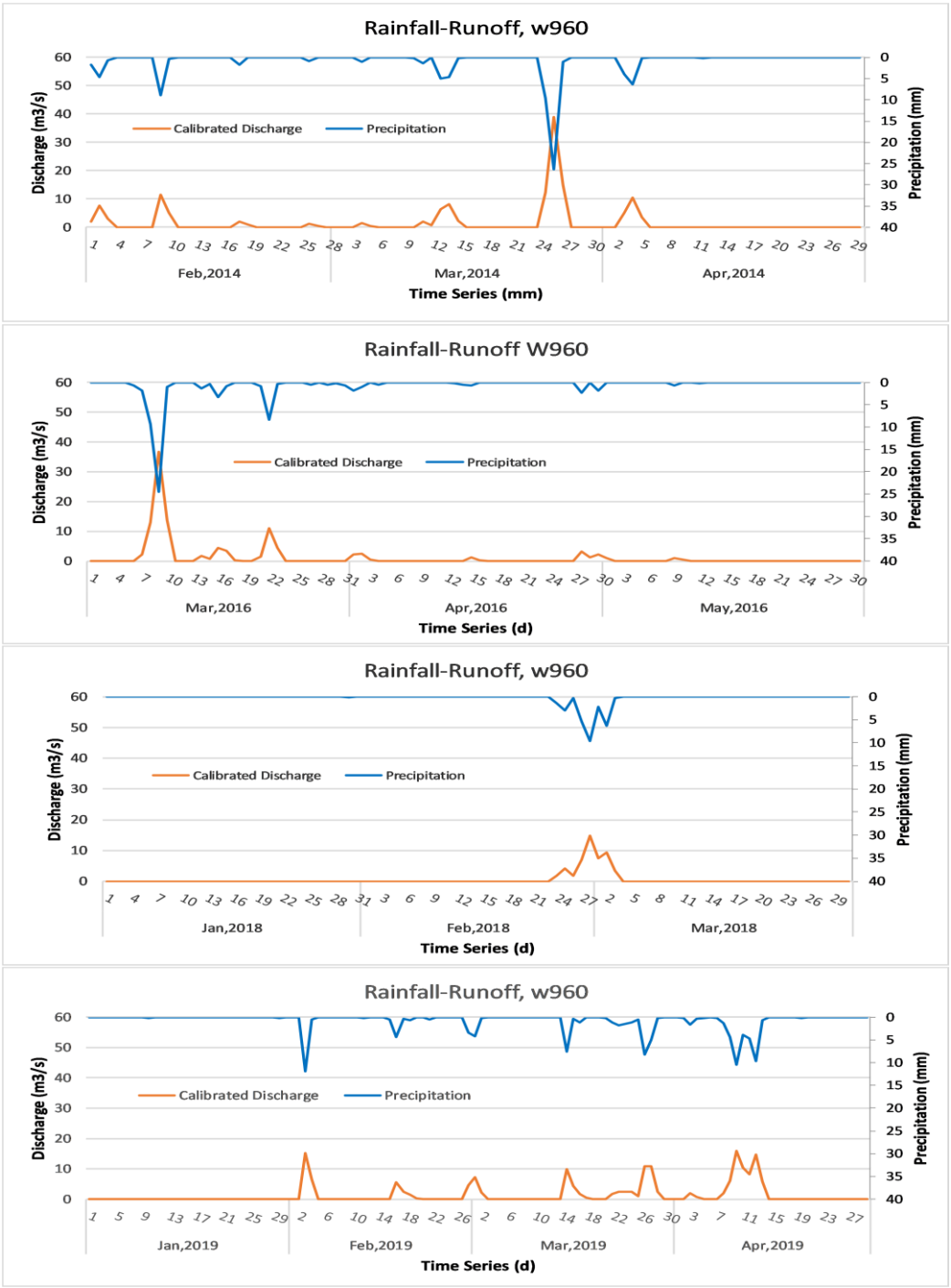

Figure 3-12*:* Precipitation, calibrated Discharge from Sub Basin-W960 at different events

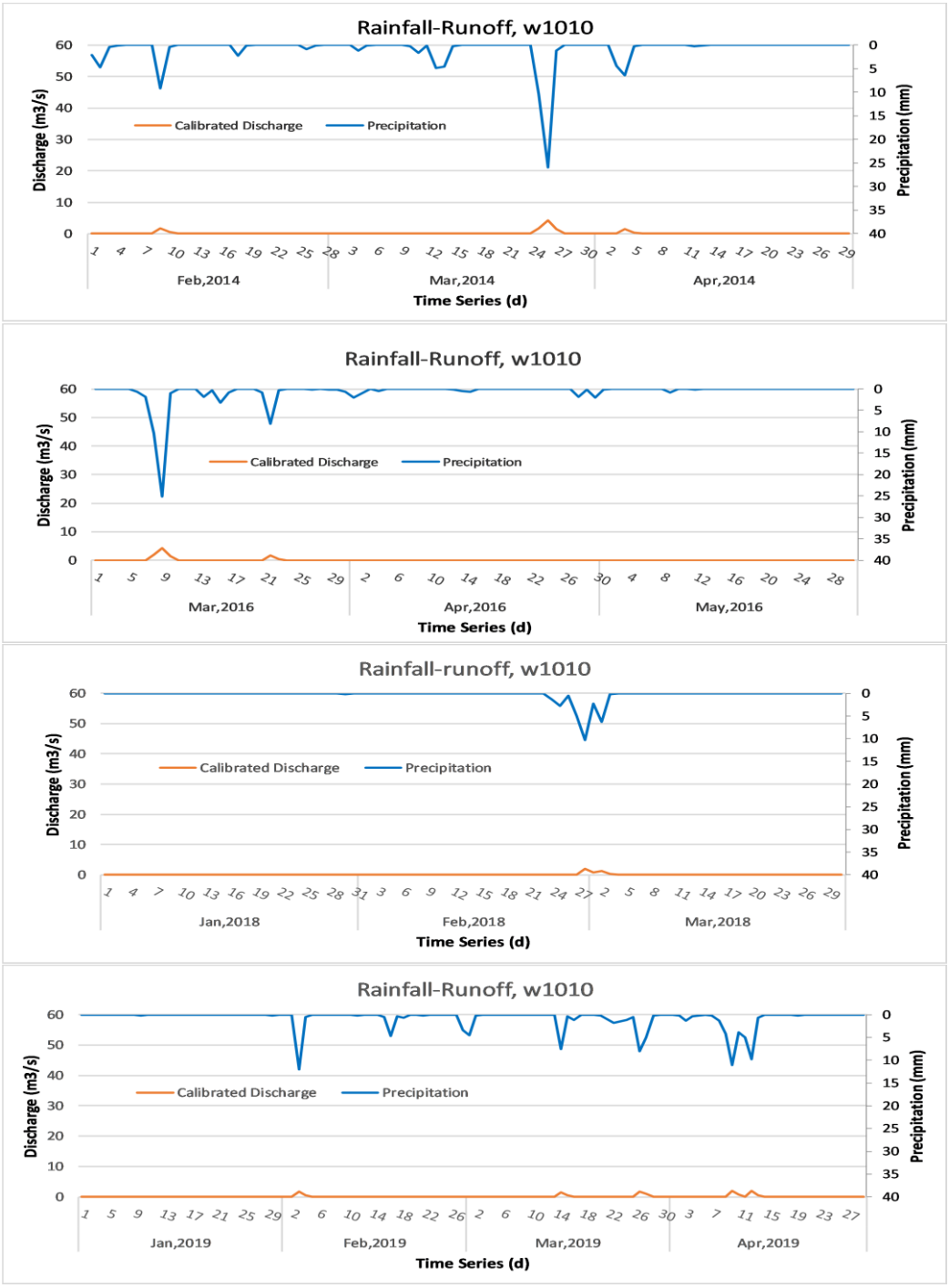

Figure 3-13*:* Precipitation, calibrated Discharge from Sub Basin-W1010 at different events

3.7. Conclusions

The HEC-HMS model is used to monitor the variability of surface runoff using remote-sensed parameters. It was calibrated and verified with Landsat images of the reservoir. This model was run using the final run processed GPM-IMERG product as a precipitation input. This product was found to be highly correlated (RMSE less than 15mm) with the ground-based measurements only in the northeastern part of the UAE, so it is recommended not to be used alone in the other areas of this region for the hydrologic and hydraulic modeling. The simulated volume of the surface runoff collected at the outlet of the watershed was compared with observed waterbody scenes by Lansat-8. With 2% of the basin area impervious, the model gave a relatively small percentile difference (as small as 8%) with RMSE of 0.24 between the simulated and the observed volume of water stored at the reservoir. With this value, this hydrological model setup is expected to be used for future studies such as water availability, flow regulation, and water management plans. Moreover, this model set up is helpful to understand the hydrological processes in this specific area or other areas with similar geomorphology and climate characteristics with the use of remote-sensed gridded precipitation, and other climate data. Nevertheless, the low amount of average rainfall, which is 80mm per annum, and the low correlation value of GPM makes this hydrological model very unlikely to be implemented in the other parts of the UAE. So it is recommended that this model can only be applied in the northern and eastern parts of the country or regions with similar weather conditions.

Preliminary results of the outflow were promising for the 2D hydraulic modeling and flood mapping of the area using HEC-RAS in this region, which is briefly discussed in the next chapter.

Phase 2

Hydraulic Modelling

Chapter 4

4. Hydraulic Modelling

4.1. River Analysis System and Flood Mapping

Floods are caused by extreme hydro-meteorological events while their evolution depends on permeability of the soil, land/vegetation cover, and the geometric characteristics of the river/wadi basins. The expansion of urban makes the more prone to flooding. From the results of simulation models, a shift in the future climate will cause reduction in the water availability in several regions. As a result, almost every aspect of human life, including production rate from agriculture, municipal and industrial water supply, energy use, wildlife, and flood control, would be affected [107]. Flood hazard estimation can be carried out using methods of varying complexity depending on the available data, time and resources [108]. Floods destroy roads, topple and wash away bridges, making some areas inaccessible. Therefore, flood mapping is found to be essential to provide important information for preparation, evacuation, and damage estimation in case flood events of similar magnitude occur again. The main goal of this part of the study is to prepare flood maps so that flood prone areas within the basin can be identified.

There are different types of one-dimensional (1D) and two-dimensional (2D) channel flows and inundation flood models. It should be stressed that each model has its own limitation arising from the numerical methods adopted and the selected governing equations. These include:

- LISFLOOD-FP

  This model adopts the diffusive wave equations, which only considers non-inertial parameters. This model is a raster-based hydraulic model, designed for research purposes especially high-resolution simulations. It solves an inertial formulation of the shallow-water equations in explicit form through a finite difference scheme [109] and [110].
- EFDC

  The Environmental Fluid Dynamics Code (EFDC) is most recent product in hydrodynamic models (a state of the art) that can be used to simulate in marine environment either in 1D, 2D or 3D. It has been widely used over the past twenty to thirty years as a hydrodynamic model worldwide. Additionally, this model utilizes the mass conservation scheme for drying and wetting in shallow areas [111].

- SOBEK

  This model is a well-known modeling tool in optimization of drainage systems, control of irrigation systems, flood forecasting, design of sewer overflows, river morphology, and surface water quality. It can describe the physical processes of network systems and horizontal grids in 1D and 2D [112].

- MIKE-SHE,

  This type of model is built on coupled physics-based models for surface flow, groundwater flow, and dynamic channel flow with inclusion of the complex feedbacks and interactions. Besides, this model also includes processes such as vegetation-based evapotranspiration, irrigation, snowmelt and water quality [113].

- WASH123D

  This model is an integrated multi process based on the computational model of various spatial and temporal scales, aiming to simulate the dendritic open channel flows [114].

- FLUCOMP

  It is designed to simulate steady and unsteady flows and can include the artificial structures built such as bridges, weirs, and spatial variations in roughness. However, it is limited to channels with water surface and their flood plains that are normal to the direction of flow. Through these settings, it is clear that this model should not be used in studies performed on the flows at or around the confluence of two major streams, where it is expected to experience a significant difference in water level [115].

- HEC-RAS

  Adopts the dynamic wave equations, which are valid for all unsteady open channel flows.

The Hydrologic Engineering Center-River Analysis System (HEC-RAS) model performs fully 1D and 2D computations by adopting the dynamic wave equations to solve the wave equations through an implicit finite-volume solution [116], [117], and [118]. These equations include all the approximation terms such as pressure gradient, effect of gravity, the local/convective inertia terms, and friction losses. The water surface profiles of the gradually varied steady flows are computed using the energy equation with an iterative procedure known as the Standard step method as shown in equation (8). This method is suitable for determining the depth at specific location in non-prismatic channels. Flood modeling can easily be accomplished using the available tools such as HEC-HMS/RAS and GIS. Once they are calibrated well, the model's results offer a reliable estimate and information that can be used in decision making by national and/or district policy makers in the country. For several years, HEC-RAS tools have been tested and are widely used globally in hydraulic modeling and flood mapping [119], [120], [121], [122], and [123]. When

developing policies for land use and management of flood plains, flood hazard maps are the key tools which can be used in decision making.

$$Z1 + Y1 + \frac{\alpha_1 {V_1}^2}{2g} = Z2 + Y2 + \frac{\alpha_2 {V_2}^2}{2g} + he \qquad (8)$$

$$he = \frac{1}{2}.\left(S_{f1} + S_{f2}\right).\mathrm{L} \qquad (9)$$

$$S_f = \left(\frac{\mathrm{nQ}}{\mathrm{A}R^{2/3}}\right)^2 \qquad (10)$$

In the equation above, $Y1$ and $Y2$ are the water depths at each cross section in meter; $V1$ and $V2$ are the average velocities in m/s; $Z1$ and $Z2$ are the elevations of the channel at each cross section in meter; $\alpha_1$and α_2 are the weighting coefficients for velocity; g is acceleration due to gravity in m/s^2; he is loss of energy head in meter. This loss is the sum of both the friction losses and the contraction and expansion losses in between the two cross sections. It is calculated using equation (9) where L is the horizontal distance between two sections and S_f is the friction slope calculated by equation (10) which is the manning equation. Q is the volume rate of flow in m^3/s; n is the manning roughness coefficient; A is the cross sectional area in m^2 and R is the hydraulic radius in meters.

Some of the flood estimation and mapping products generated with different techniques carried out around this region are the Flood hazard maps in the agricultural areas of Uganda[124], the automation of terrain modeling and floodplain delineation in the semi-arid regions of Iran [120], and also the Weather research and forecasting (WRF) model used by Deng et al. [125] to investigate the effect of model resolution and parameterization on the simulation of flood-causing events in Saudi Arabia. Furthermore, Al-Zahrani et al. [126] showed the efficiency of HEC-RAS on quantifying the flood hazards in the city of Hafr Al-Batin, in Saudi Arabia. In Tunisia, the extent of the depth of the flood hazard through the flood mapping of a specific event, which had caused serious effect on the plain areas, was studied by Ezzine et al. [127]. Owing to the ability of HEC-RAS to model hydraulic channel flows that range from simple single reach models to complicated networks, the hydraulic simulation of wadi Ham is performed in this paper. This simulation was helpful in generating the maps of maximum flood depth and velocity, which can be used to identify the flood prone areas and play a major role in planning. Furthermore, this could aid in further predicting the occurrence of such floods in the future.

4.2. Methodology, Discussions and Results

In the previous phase of this project (Hydrological modelling part), it has been noted that routing techniques are classified into two categories: hydraulic and hydrologic routing.

i. Hydrologic routing (HEC-HMS): flow is calculated as a function of time only. It employs not only the continuity equation but also the analytical or empirical relationship between the storage within the reach and the discharge at the outlet.
ii. Hydraulic routing (HEC-RAS): flow is calculated as a function of both space and time. It is governed by the partial differential equations for the unsteady non uniform open channel flow.

These partial differential equations are referred to as the Saint-Venant (momentum) equations or the dynamic wave (diffusion) equations [128] and [129]. The Saint-Venant equations are used to represent the transient flows in an open channel [130]. They are applied mostly in gradually varying open channel flows [131]. They are derived from the Navier-Stokes equations, and include the pressure gradient, gravity effect, local inertia, and friction losses as shown in equation (11) [132]. On the other hand, the diffusive wave flow equation only include the effects of the pressure and friction losses without accounting for the local or convective inertial terms. According to a study performed by Ponce et al. [133], the bed slope and wave period are important physical characteristics in determining the applicability of the undermentioned equations in model preparation. Some of the application of these equations in models include: channel constriction and obstruction issues [134], the movement of particles along potential flow streamlines through junctions [135], the effect of gravity for waves reduced by sudden flow stoppage [136], and the storm-induced flash flood routing in a surface flow, what this study focuses on.

HEC-RAS, the hydraulic simulating model, is able to simulate any stream or wadi systems ranging from simple single reach models to complicated networks. The HEC-RAS version 5.0.7 with 2D modelling was adapted in this study. This model has the capacity to solve the 1D and 2D hydraulic flows either using Saint-Venant equation (Momentum equation) or the diffusive wave equation. Even though both methods give the same result, for the 2D, solving the simulation using diffusive wave equations simplifies the full dynamic wave equations at a faster rate. Besides, Yen and Tsai [137] demonstrated that “diffusion wave can be mathematically formulated from different levels of shallow water wave approximations assuming that the celerity and coefficient of hydraulic diffusivity are step-wise constants”. Thus, in this case the 2D diffusive wave equations were used for the unsteady flow analysis. The 2D hydraulic model based on diffusive wave equation is a non-

linear system, which is mainly a conservative form ensuring consistency with the mass conservation principle as shown in equation (12).

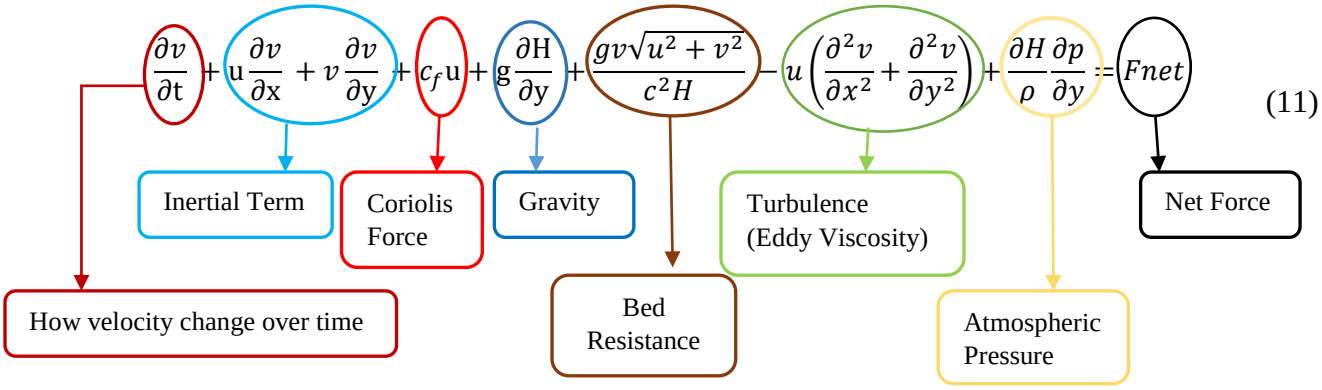

$$\frac{\partial H}{\partial t} - \frac{\partial}{\partial x}\left(Kx\frac{\partial H}{\partial x}\right) - \frac{\partial}{\partial y}\left(Ky\frac{\partial H}{\partial y}\right) = Fnet \qquad (12)$$

$$\Phi = P - I - E \qquad (13)$$

where: t is the time (s); x and y are the space coordinates (m); H is water surface elevation above the datum (m); Kx and Ky are hydraulic diffusion coefficients; Φ is the storage (mm); P is precipitation (mm); I is infiltration (mm); and E is evaporation (mm).

Recent studies suggest that the uncertainties coming from the incorrect interpretation of flood dynamics and unrealistic models of the terrain topography can be minimized using 2D models [138]. Furthermore, hydraulic simulation models, such as HEC-RAS, are able to compute sophisticated equations. The deployment of 2D modelling software, in combination with high-resolution digital elevation models, has become more viable for hydrologists, researchers and engineers [138]. Some studies, however, point out that for the large-scale studies, coarser resolution DEMs, greater than 100m, decreases the reliability of the 2D model simulation outcomes [139]. The same study showed that terrain obtained from DEM of 50m and higher spatial resolution, will not be effective in producing probabilistic flood mapping products. From Shustikova et al. [123], HEC-RAS 2D modelling using the high resolution (1m) DEM showed better result for the estimated flood extent and water depth in Secchia River in Italy. According to Haile and Rientjes [140], 2D flood modelling using LiDAR data for urban areas require high-resolution data (not more than 15m) and concluded that resolution of the DEM affects the model output significantly. Bearing this in mind, for this study, the author was not able to get a much finer resolution DEM less than 30m.However, this DEM is not pixilated for bare land and there are only few buildings

with farm lands in the study area. From the total area of HAM basin, 193km^2, the selected area of flood zone for the 2D flood simulation is only 28.3km^2 as shown in *Figure 4-1*. The DEM of the study area was projected, clipped and masked in accordance to the boundaries of the HAM basin. It is to be noted that the same DEM was used in generating the runoff in the hydrological simulation model with the gridded precipitation data from GPM-IMERG mission as discussed in Chapter three. Once this DEM was imported in the HEC-RAS simulating software, the terrain of the area was prepared after setting the exact geographical reference of the DEM. To check whether the DEM exactly superimposed within the study area, web imagery layer was added to the terrain developed.

To perform the computational analysis for any hydraulic modelling, geometric calculation is the first step. The geometry data accounts for the shape, size and stream cross section network (connection). Using the finite element method/analysis, a mesh/grid for the flooded zone was developed within its boundary region. The smaller the cell size of the mesh, the more accurate the calculation will be. Accordingly, the total number cells in the mesh were considered to be only 70,747, with the average area of each cell equal to 400m^2, as the dx and dy are specified to be 20m, smaller than the grid size of the DEM used. This mesh size is considered with regards to the study performed by Fewtrell et al. [141]. In their study, the 2D models' behavior was strongly affected by the heterogeneity of the area (building, roads, natural river course, farm land), and requires a very fine mesh to represent the building dimensions and show the effects of the final result within that area.

Another major factor affecting the hydraulic flow of the river is the roughness coefficient, which mainly depends on the land cover type. The channel of the wadi is mostly bare sandy soil. However, there are small towns with relatively different roughness coefficients near the course of the wadi. Visual inspection using Google Earth and the areal imagery helped to infer the nature and type of the soil and land cover, and compare them with that obtained from MODIS satellite. For each type of land cover, estimation of Manning's roughness using the Chow's tables [142] was possible after the land cover data (image by MODIS) of the area was imported in HEC-RAS mapper. Furthermore, McCuen [143] discussed the values of Manning's roughness coefficient for different area types.

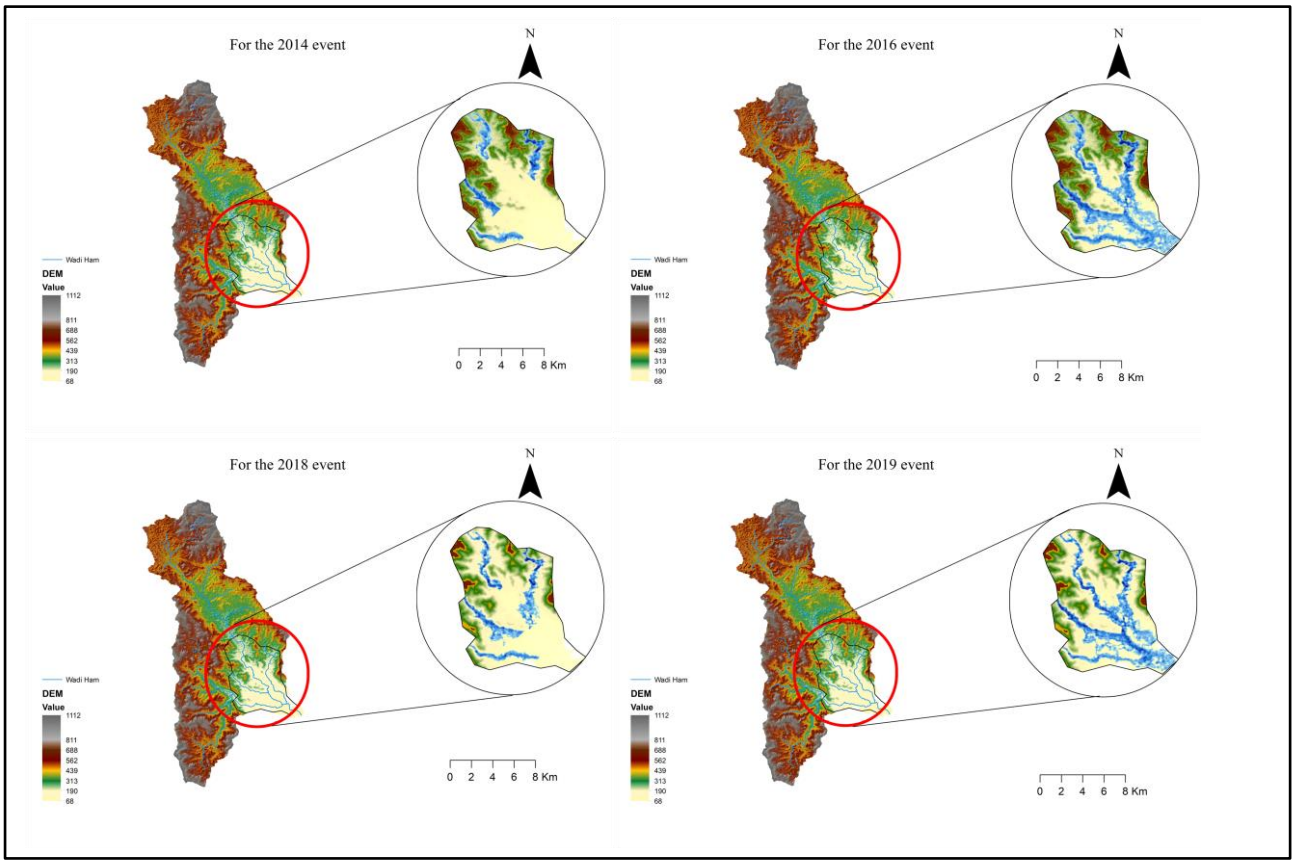

Figure 4-1*: The maximum runoff generated at different events in the flat lowland plains of HAM basin: Top left:23 Mar- 30 mar, 2014; Top right: 05 Mar -25 Mar, 2016;Bottom left: 22 Feb-07 Mar,2018; Bottom right: 14 Mar-16 Apr,2019.*

The Terra and Aqua-Combined MODIS land cover type (MCD12Q1) version 6 data product provides global land cover types at yearly intervals on a daily basis 500m spatial resolution [144]. This version is derived using the supervised classification of MODIS Terra and Aqua reflectance data. Hence, this land cover data is used as per the existing land type in which only five classes matched in this area. These include built up area, mountainous, barren soil, vegetation and water body. Basically, Manning's value estimates for natural channels from USGS online data were selected based on the physical characteristics of the channel. It is a fact that the roughness coefficient is expected to change from one area to another area, even for the same river (the surface profile and roughness of the ground). Hence, the author has assigned the Manning coefficient to each class based on the land cover type. This will have an effect on the overall simulated flood depth and velocity.

The second and most important process that was performed in this computation is the 2D unsteady flow analysis, which basically refers to the volume of the runoff and setting up of the boundary conditions of the flow. Two types of boundary conditions, namely the flow hydrograph boundary

conditions and a normal depth boundary condition, have been adopted in this study as shown in *Figure 4-2*.

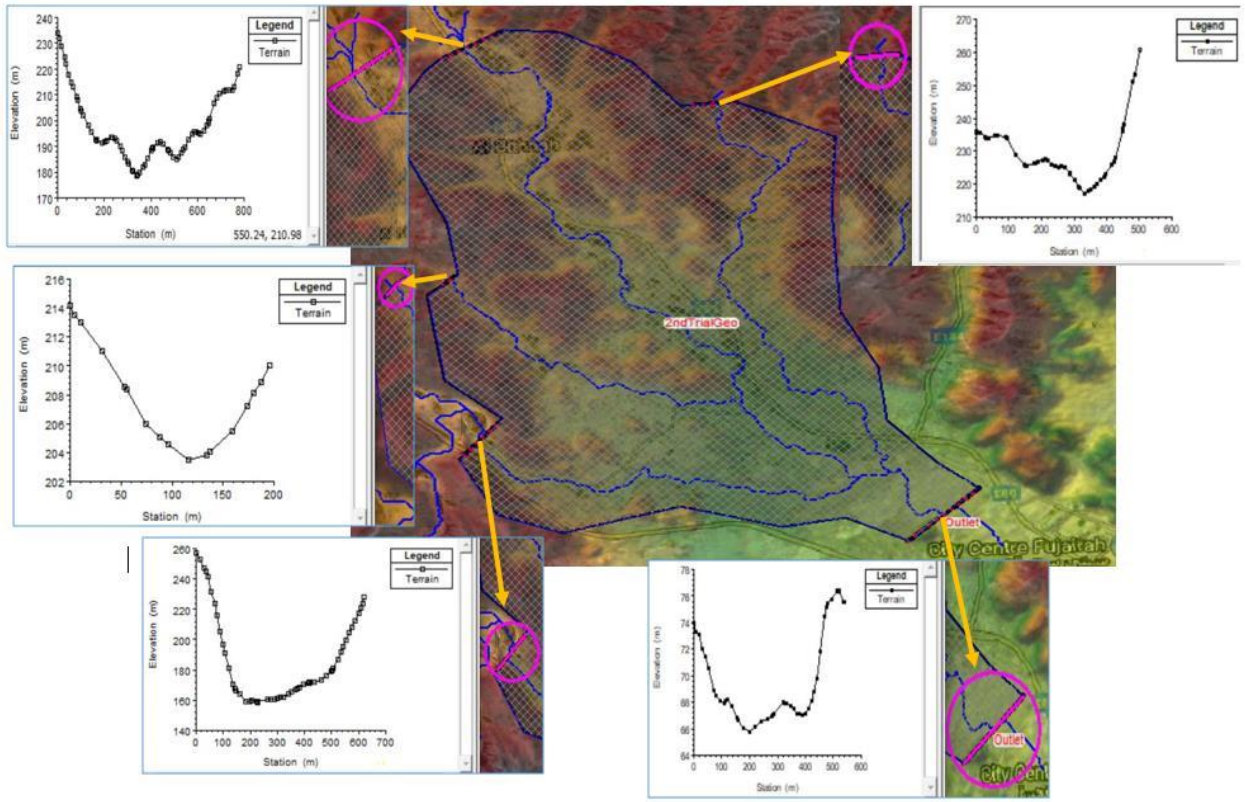

Figure 4-2*: Photo taken from Geometric analysis in HEC-RAS. The profile of boundaries is shown by indicating the location of 4-inlets and an outlet boundary in the irregular polygon (colored one) of the floodplain zone in HAM basin*

The four upstream hydrograph boundary conditions, each with energy slopes of 0.02 for Up1 and Up2, 0.04 for Up3 and Up4, and an outlet with normal depth having a frictional slope of 0.006, are shown in *Figure 4-2*. These slopes are calculated based on the geometric profile (dy/dx value obtained from their cross sections in the topography). A normal depth is estimated based on the energy slope used where this slope is approximated as the average slope of the channel at that cross section. Besides the flow hydrograph, the energy gradient has to be defined for the four upstream (inlets), as this is used for distributing the discharge over the cells which integrate the boundary. This distribution was based mainly on the stated slope and the pre-processed hydraulic properties of each cell. Since there is a dam constructed at the outlet of the basin before it enters the city of Fujairah, the downstream boundary/border of this hydraulic model was considered at the section of the dam such that the total simulated flood was accumulated within this area. The findings of Haile and Rientjes [140], proving that 2D flood modelling using LiDAR data for areas with artificial structures such as building, highways require high-resolution data (maximum 15 m grid size) gives such an accurate simulated flooding flow, was taken into consideration.

In this study, four events were considered. Since the discussion and results acquiring methodology is the same for all, a 2016 event scenario is discussed in detail to highlight how the flood flows throughout the basin and its effect on the built up areas located near the periphery of the wadi channel. From the discharge flows generated in HEC-HMS for the storm event from 05March to 25March 2016, the peak flows in the runoff hydrograph and used as input in the HEC-RAS model. The unsteady 2D flow computational analysis was performed with a computational time interval of every 1hour. Once the computation was performed, the unsteady flow was simulated. The maximum flood depth and water surface elevation (WSE) maps were generated for the specified flood plain of the Ham basin as shown in *Figure 4-3*.

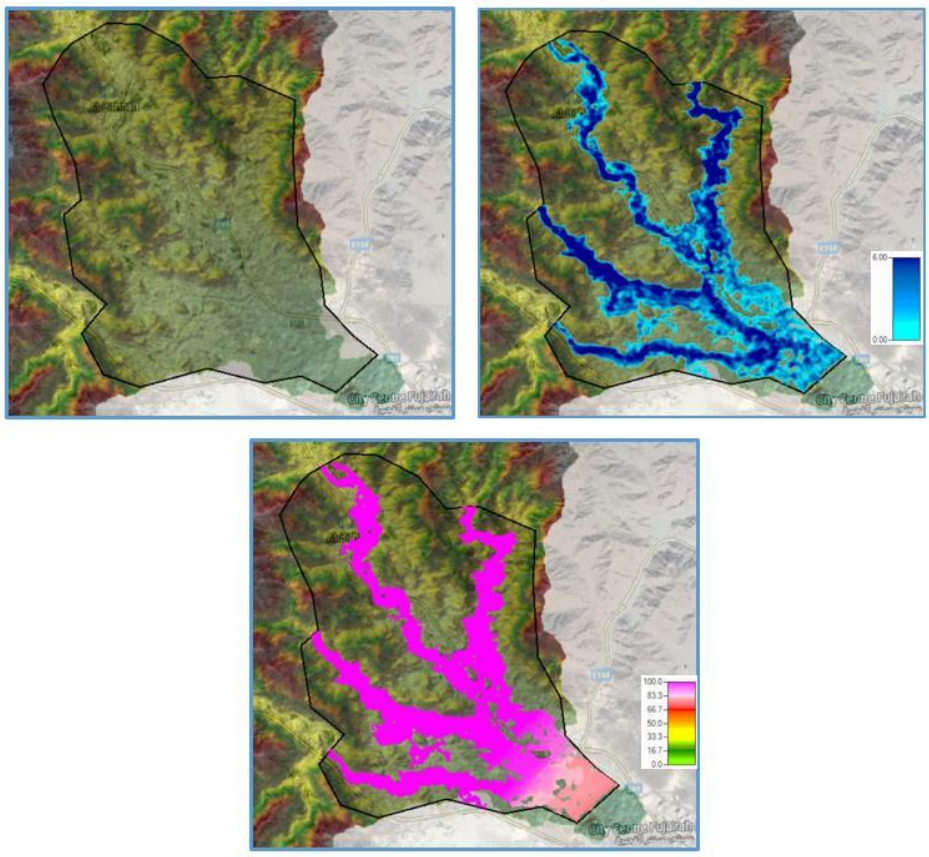

Figure 4-3: Flood plain selected for the HAM basin in 2016 event: without flood(left), with Max flood depth (right) and max WSE (the one with pink color)

From the results of the simulation, the maximum depth of the flood reached 6m, flowing at a faster rate at the narrow gorges and steeper areas and slowing down with the shallow depth of the water level when it reached the level area after crossing the Rinawi farms. The flood depth varies from point to point because of the topography of the area, and was calculated by taking the difference of the water surface elevation (WSE) and the digital elevation of the area. According to the diffusion model equation, this storm event was able to inundate the southern part of Al Bitha (extreme upstream part of the wadi within the selected area in *Figure 4-3*) and the farm lands around during

its the maximum level measured on 20 March 2016 in the afternoon. Furthermore, the Rinawi farms and some residential areas around it, located 4km south of Al Bitha, were also found to be vulnerable to the flash flooding as shown in *Figure 4-4*. It should be noted that the scale used for the simulated flow and the areal image of the area in *Figure 4-4* is not the same. Since the DEM used was not finer than 15 m resolution, the output of the model was significantly affected. The model has exaggerated the depth of water as such, the water is simply passing over the built up area. This shows, the model could not identify the artificial structures such as building from the natural terrain as such the walls of the buildings could not prevent the incoming flood even if the depth of the flow was lower than the height of the retaining walls.

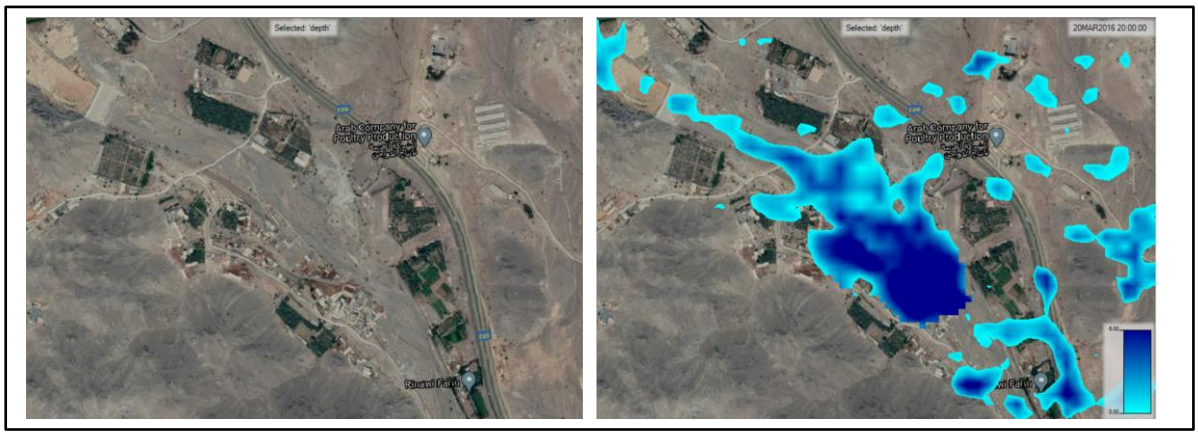

Figure 4-4*: Residential Zone around the Rinawi farm without flooding (Left); when flooded (Right)*

The figure above clearly illustrates that the model was unable to identify the artificial structures such as building, levees (provided for roads). Given this, the flood was simply following the contour of the natural terrain and resulted in the overflow of the flood to all the buildings on its way. Hence, it is somehow impossible with the DEM used to capture important local topographical features, such as channel embankments or levees, and the thin compound walls of the building, especially when the linear features are significantly narrower than the model resolution. This limitation is discussed by Shustikova [123]. Furthermore, it was noticed that there is certain amount of hydraulically disconnected flooded areas. As such, the flood was seen to simply enter the built up area even though the height of the thin boundary walls of the building was high enough to block the flood from doing so. From the literature and the manual of HEC-RAS, such limitations similar to those discussed by Shustikova [123] can be solved either by refining the mesh with break lines, reducing the mesh sizes along such linear irregularities, or using finer DEMs as mentioned previously. However, in this study the refinement did not bring a worthy result, and hence the author

recommended the use of a finer spatial resolution DEM (mostly 1m) so that this flood mapping can be later extended to the urban area.

4.2.1. Analysis of Water Surface Profiles and Surface Elevation

Several cross sections have been selected on the main and tributaries of the wadi Ham for visually comparing the water level and surface elevations in the model simulation during the different events. As noted before, there was no stream flow gauging station within this wadi that could be used for verification of the model performance. However, these simulated stream flow hydrographs of each sub basin (generated used HEC-HMS) were already calibrated and verified using Landsat images for the total volume of water collected in the reservoir. The extracted surface areas captured by Landsat were used as a proxy for verifying the simulated runoff/volume of water. Using the calibrated hydrographs as input to the hydraulic modelling (HEC-RAS), a longitudinal profile of the maximum water surface elevation for the events of 2014, 2016, 2018 and 2019 was generated, as shown in *Figure 4-5*. This figure shows the simulated water surface elevations on the main channel of wadi Ham extending for about 11km from Al Bitha area in the North towards the Ham dam located in the south passing through the Rinawi farm.

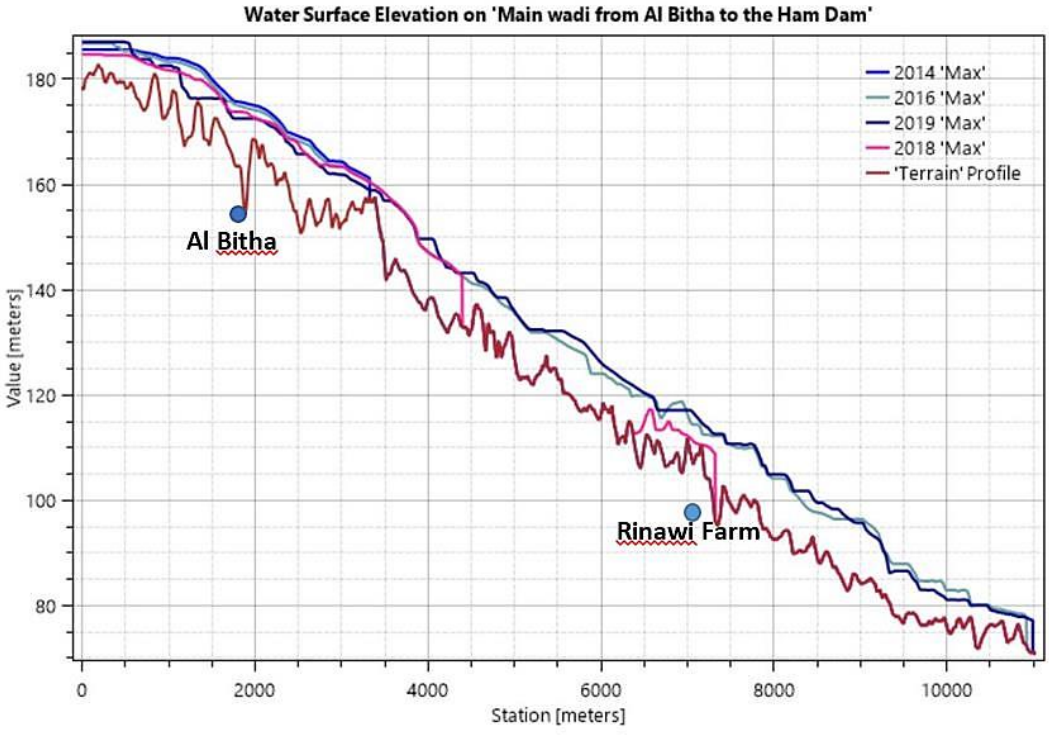

Figure 4-5*:* Water surface profile of different flood events in the main Wadi segment from Al Bitha to Ham dam

It is clear that whenever there is heterogeneity on the wadi bed and slope, it is very difficult to estimate water flow rates during both flood and non-flood periods, as illustrated in *Figure 4-5*.

Through *Figure 4-6*, it is easier to identify clearly where the cross section of each profile (shown in *Figure 4-7*) is located. The profiles of simulated water levels at various cross sections of the wadi within the selected flood plain shown in *Figure 4-7* point out that there was higher flow during the 2016 and 2019 events. As can be seen, the water levels exceeded the wadi banks in most sections during all the events, indicating a situation of precarious concern in the downstream area. The profile of the wadi channel in this area is mostly wide and somehow shallow, as the water flows uniformly over a bigger area and is not limited to a specific path, in a smaller magnitude flow. In general, this sectional profile helps to easily visualize the depth of the maximum water level in each section by identifying points/areas with higher depths using the WSE. It should be made clear that the WSE used is the cumulative runoff within the events considered, i.e. the maximum possible depth which can occur. If a specific event of the runoff for a day or two were to be used, the depth of the water flowing would be a few centimeters at almost all the sections.

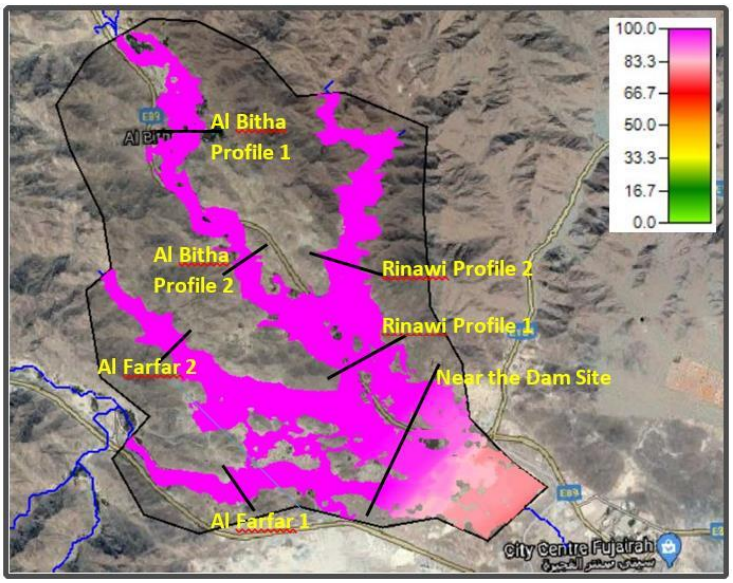

Figure 4-6*:* Top view of the Profile Cross sections for the water surface profile during the 2016,2018 and 2019 flood events in the lowland section of the Wadi Ham (scale used is in meters)

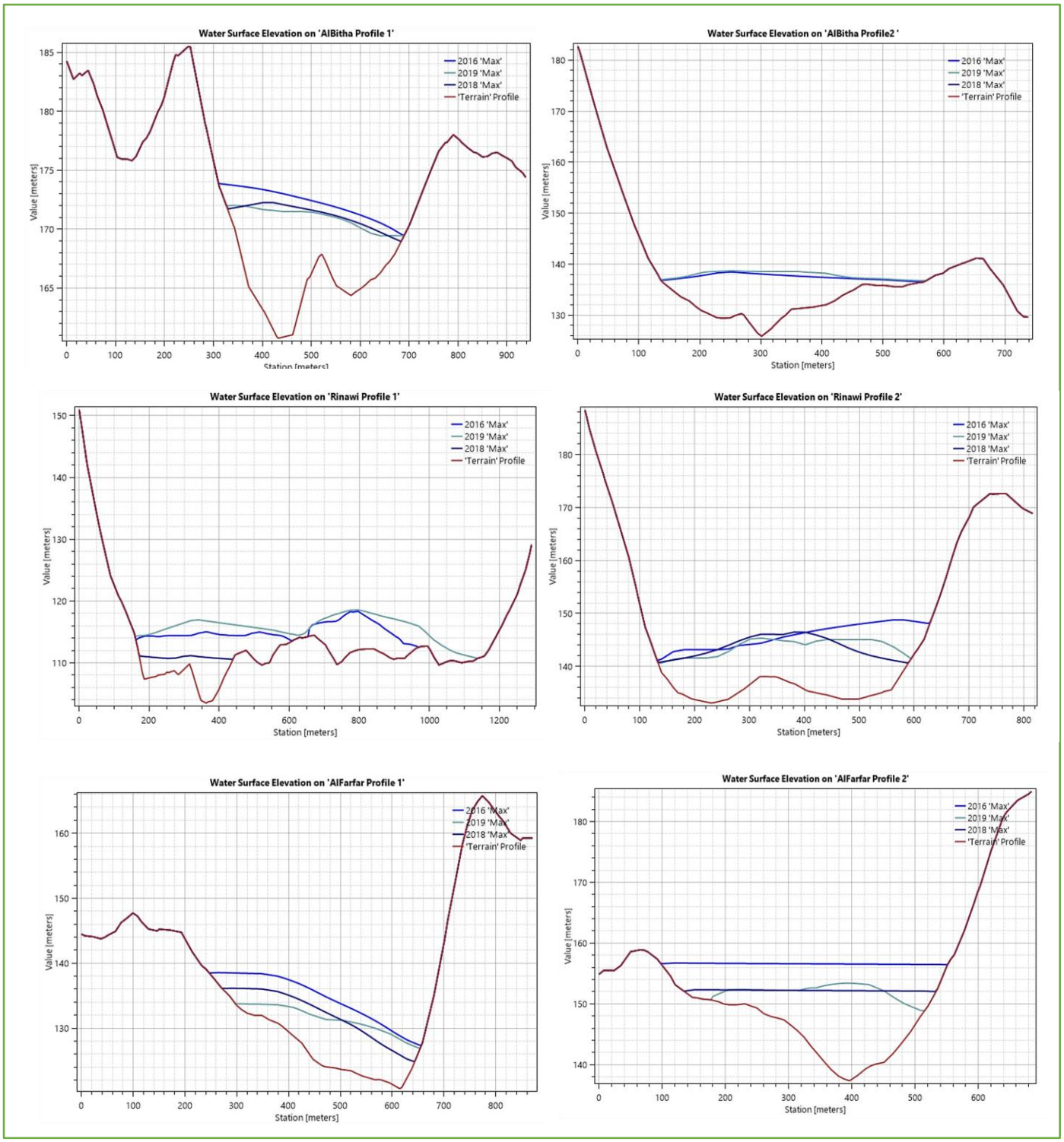

Figure 4-7: Maximum WSE on the selected sections of lowland part of wadi Ham during specific months of 2016, 2018 and 2019 rainfall events

4.2.2. Flood Hazard Mapping

The flood water depths were classified into flood hazard categories, so as to prevent damage for the property and mainly loss for mankind according to the Japanese criteria of the Ministry of Land Infrastructure and Transport (MLIT) [145]. This classification is mainly used when flood mapping is performed in urban areas. According to this criteria, "there are five flood hazard categories. Flood hazard H_1 (flood depth lower than 0.5 m), known as very low hazard, meaning that the flood does not pose any risk to people and on foot evacuation is possible. Flood hazard H_2 (flood depth between 0.5 m and 1 m), known as low hazard, mean that flood water could pose hazard for children and on foot evacuation can be difficult. Flood hazard H_3 (flood depth between 1 m and 2 m) is defined as medium hazard. In this classification, the water depth has the potential to drown people. For a flood depth between 2 m and 5 m or higher, a hazard normally represented by H_4, there is potential to put people at risk, even when they are inside their houses. The life-threatening hazard is H_5 for a higher depth of flood, which could topple man-made structures completely, and there is a higher possibility of people drowning."

The above flood classification was performed in this study area not because the selected area is concentrated with residential building and to alert the municipality to take major action, but to give an insight on the depths of the water level at different sections of the runoff. *Figure 4-8* shows the flood hazard map of the study area for the 2014, 2016, 2018 and 2019 events. All the extreme flood hazard cells (level H_5) are located within the wadi channels at sections with deep depth (like gorges). It should be noted that all these values of the flood depth are the cumulative values of the event considered (not of a specific day or hour). In the 2016 and 2019 events, the flood hazard levels surrounding the Rinawi farm were found to be in the range of category H_3 and H_4. Considering the location of the farm, on the periphery of the wadi path, there was overflow of the water towards the farm area. The residential buildings within 300m to the west of the farm were prone to the H_3 flood hazard category. Thus, for similar events, evacuation measures can only be implemented to the west of these buildings as there is very low flow in that direction. The flat plains of Ham basin near the dam showed prevalent flood extent with classification from H_1 to H_3. Although there is no city nor town located on these Ham basin plains, these plains are not deserted: there are agricultural activities and some industries. Therefore, building levees for redirecting the water to other directions is one of the best solutions, to mitigate the effects of the flash floods which have the capacity to threaten the continuity of the farming and other activities in the area. *Figure 4-8* illustrates that the simulated flood water level is significantly higher than normal in the wadi channel, and that in the banks it also reached depths up to 2m at specific areas as discussed above.

From the simulated hydraulic flows and water depth maps, the area of inundation for the spilled water over the banks in both sides is relatively high throughout. Hence, the author strongly recommends deploying gauging stations to deliver warning messages after measuring the outflow depth, and communicate with the regional and local government offices to minimize the effects of such natural disasters.

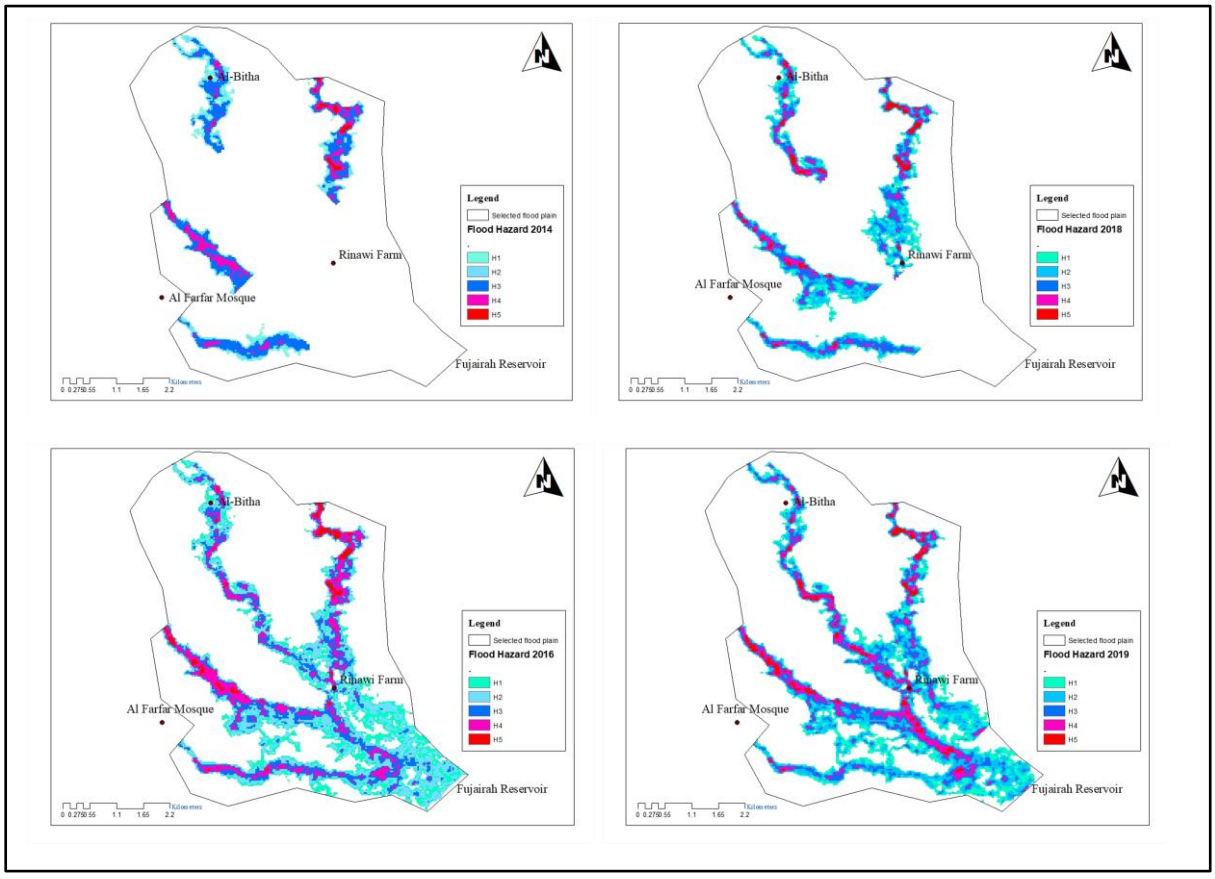

Figure 4-8: Flood hazard Map according to the classification [145] considered

As a possible solution for mitigating the flash flooding in this region, the construction of small dams in a cascade form at certain sections of the wadi is a feasible option. This way, the depth and volume of the flood carried by the wadi from the higher land will be reduced, and its impact on the downstream agricultural and built up areas will be highly minimized. In addition, constructing retaining structures, such as levees for diverting the water flow is found to be necessary.

4.2.3. Validation of the model

Cloud-free flood images represent a reliable and continuous data source for the evaluation of flood inundation model simulations. For instance, the daily MODIS flood maps are used for the validation of the simulated models. Unlike other sources such as Landsat (16 day), ERS-2 SAR (35 day), and ENVISAT ASAR (35 day), they don't suffer from latency and temporal availability-related

problems. The scope of this work is to validate the flood maps produced from the hydraulic model with the resulting cloud-free flood images/maps.

To detect flood pixels, [146] employed the MOD44W product version 6 [147] as a reference water covered layer (i.e. depending on the coincidence of the water-covered pixel with MOD44W). Similar to Tran et al [148] study, bands 1 (red) and 2 (NIR) at 250m spatial resolution of NASA's MODIS Surface Reflectance version 6 products, MOD09GQ/MYD09GQ [149], were used in this study. These bands are mainly used in land, cloud, and aerosol investigation. The bandwidth ranges from 620nm to 670nm for band 1, and from 841nm to 876nm band 2, with a common value of 21.8W/m^2 for spectral radiance. Only a few images were found to be cloud free around the time stamp used in the model simulations. After selecting those images, and based on the results of the reflectance ratio of NIR band to Red band , pixels were considered as water when the ratio of NIR to red in these cells is less than 0.7 [148].

The geometric area within the delineated boundary of the flood zone of the study area is 28.3km^2. This is much too small to get a sufficient number of pixels from MODIS (the average number of cells is 450 with grid size equal to 250m by 250m horizontally) for the water body during the flood event. Hence, the author was unable to extract pixel with water (the path of the runoff) with a reflectance ratio smaller than 0.7. Alternatively, images captured by Landsat (30m spatial) were considered, despite their coarser temporal resolution (16day), for validation of the simulated flood maps. These images are considered to be, more than eight times higher resolution (spatially) than MODIS. The path of the water (flood) is indicated with a unique color after classifying the different values of NDWI. It is known that the NDWI index was based on Landsat-8 green and near-infrared bands (band 3 and band 5, respectively) [103]. However, the time stamp for most of the images captured by this satellite did not match with the simulation time of the flood, and the remaining images were not cloud free. This is basically due to the low temporal resolution (16day) of the Landsat images (captures two images in a month at most). Hence, the considered cloud free images captured by the Landsat cannot be used for validating the simulated flash flood maps. Hence the author came up with the following two concluding points:

a. Temperature, land cover and imperviousness of the soil were considered in the runoff hydrograph generation during the hydrological modelling with HEC-HMS. Afterwards, the simulated volume collected at the outlet section of the basin was calibrated using the observed surface volume of water collected in that section (dam) using Landsat images. The final results were acceptable with minor differences. Hence, the author considered that the simulated flood flows and maps created using the calibrated runoff hydrograph can partially

give an insight about the extent of the flood flow that occurred during those events. However, it should be noted that the flood depth shown *Figure 4-8* is high not only because the DEM used for terrain development was at a coarse resolution, but also because the flood depth considered is the maximum (cumulated) value.

b. If the cloudy patches on the images captured by both MODIS and Landsat can be removed, the true observed flood maps during the rainfall event could be obtained and subsequently used in the verification process by comparing it with the simulated runoff maps. Otherwise, ground based measurements for the observed flow will likely be required.

4.3. Conclusions

The unsteady wadi flow, in the selected four events, generated from hydrological modelling using HEC-HMS and subsequently calibrated and verified by the Landsat images was used as an input for the hydraulic modelling in HEC-RAS. Besides, land cover was employed in the estimation of the Manning roughness coefficient, and the DEM for the terrain profile. Several maps have been prepared for the maximum flash flood inundation during those events. Results of the 2D hydraulic modeling and flood mapping of the area were somehow promising at a preliminary stage. A comparative analysis performed between the simulated flood flow maps and satellite images such as MODIS and Landsat for the validation and efficacy test of the model was not successful as discussed in section *4.2.3*. On the other hand, there are three major obstacles that prevent the application of this hydrologic and hydraulic model not to be implemented elsewhere in the UAE:

i. The low precipitation values; as in most part of the UAE the average rainfall per annum is below 80mm;
ii. The unavailability of finer resolution DEM (<10m) for this region;
iii. For such small areas considered, spatial resolution of GPM precipitation product (0.1^0) is coarser as it underestimate/overestimate the rainfall in the wet and dry part of the basin.

In general, the author believes that the setup of the hydrologic and hydraulic simulation models can be improved and later on extended towards the northern and eastern part of the country if and only if the above requirements are taken into account.

4.4. Recommendations for Future works

Drylands are areas with limited water systems categorized by a spatial and temporal variability of rainfalls. The lack of finer resolution (spatial and temporal) detail on rainfall distribution from satellites posed a major obstacle for hydrological modelling. The disaggregation approach is a

solution for such kind of problems of rainfall data. It is evident that in hydrologic and hydraulic modelling, rainfall data should be at a higher spatial and temporal resolution especially in arid areas where there are spare rain gauges. Satellite Precipitation products such as TRMM and GPM are on global scale with a spatial resolution of approximately 25km and 10km respectively. So a single pixel (cell) of these products is expected to cover a large area. Therefore, a certain standard method for disaggregating the satellite-based precipitation data sets to a finer resolution (spatial and temporal) is required to be used in hydrological modelling. Therefore, the downscaling is performed in a way that these satellite products will not overestimate or underestimate the precipitation value when compared with the ground measurements beyond a certain limit [150], [151]. Let us see some of the many studies performed on developing techniques of spatial and temporal disaggregation of Satellite Precipitation products.

Tarnavsky et al. [152] brought an approach of deriving an hourly rainfall intensity with a 1km spatial resolution from a monthly TRMM precipitation datasets (0.250 grid cells). Through this study, they developed a novel approach for Fractional cover of rainfall (FCR) correction of TRMM 3B42 and simulation of rainfall fields through gamma distribution parameters in the arid areas of Senegal and Tunisia. The commonly occurring convective storms in this arid area cover only a small area of approximately 7km^2 [153], so a TRMM grid cells (0.25^0 x 0.25^0) is likely to include both the wet and dry area. As a result, the rainfall grid shows a lower rainfall intensity than the actual intensity in the wet areas and vice versa. Such scenarios lead to non-reproducible runoff in hydrological modelling. Thus FCR correction is able to increase rainfall intensities considering the FCR within TRMM 3B42 grid cells. For instance, 1 mm/hr with FCR of 0.50 (at a given time the wet pixel is 50%) will result in 2mm/hr rainfall intensity for the wet pixels

Lopez et al. [154] introduced a new downscaling methodology using the multi variable Geographically Weighted Regression (GWR) algorithm. This method adopts four environmental regression parameters (slope, elevation, EVI, and aspect) which vary with location. In their study, four satellite-based precipitation datasets, PERSIANN, TRMM, CMORPH, and MSWEP, PERSIANN, and TRMM, were downscaled from 25km to 1km. These products were tested in the in the Magdalena River basin of Colombia. Chen et al. [155] also implemented this GWR method for the disaggregation of a monthly TRMM 3B42 (0.25^0 grid cell) in the semiarid/arid areas of Gansu province of China. They demonstrated that this method was very effective in obtaining a monthly 1km TRMM precipitation with high accuracy.

Thus as a recommendation for future works,

1. Developing such disaggregation of the satellite precipitation products is very important since discharge simulations are very sensitive to the spatial resolution of precipitation datasets. Therefore, such downscaling procedures could make the global available satellite based precipitation dataset as an alternative to ground measured data in hydrologic and hydraulic modelling especially in areas such as the UAE with poor gauging networks.
2. DEM with finer resolution (<10m) has to be used in the 2D simulation to avoid the uncertainty of the hydraulic modelling. This way the effect and depth of the water level within the built up areas can be correctly identified, and animations for visualization can be easily developed. This in turn will help to identify the vulnerable areas for flash floods during similar events.
3. Reinstallation of gauging instruments along the wadi channel and use of high temporal and spatial resolution satellite images for validation purposes are necessary. The measured flow depth could be directly used in the validation of the simulated flood flow maps for getting a higher efficacy model.

References

[1] M. Khalil and A. Hammadi, “Assessment of Groundwater Resources Using Remote Sensing and GIS,” UAE University, UAE, 2003.

[2] MAF, “Climatological data,” vol. Vol 4, no. 1992–93 to 1999–2000, 2001.

[3] A. Aldababseh, M. Temimi, P. Maghelal, O. Branch, and V. Wulfmeyer, “Multi-criteria evaluation of irrigated agriculture suitability to achieve food security in an arid environment,” *Sustain.*, 2018.

[4] U. M. of Energy, “Third National Communication Under the United Nations Framework Convention on Climate Change,” *Moen. Abu Dhabi, UAE*, 2012.

[5] O. Branch, A. Behrendt, Z. Gong, T. Schwitalla, and V. Wulfmeyer, “Convection initiation over the eastern Arabian peninsula,” *Meteorol. Zeitschrift*, 2020.

[6] Y. Wehbe, M. Temimi, and R. F. Adler, “Enhancing precipitation estimates through the fusion of weather radar, satellite retrievals, and surface parameters,” *Remote Sens.*, 2020.

[7] K. N. Kumar and T. B. M. J. Ouarda, “Precipitation variability over UAE and global SST teleconnections,” *J. Geophys. Res.*, 2014.

[8] T. S. MOHAN *et al.*, “On the investigation of the typology of fog events in an arid environment and the link with climate patterns,” *Mon. Weather Rev.*, 2020.

[9] G. J. Steeneveld *et al.*, “Observations of the radiation divergence in the surface layer and its implication for its parameterization in numerical weather prediction models,” *J. Geophys. Res. Atmos.*, 2010.

[10] U. S. G. Survey, “Where is all of the Earth’s water?,” *NOAA*. [Online]. Available: https://oceanservice.noaa.gov/facts/wherewater.html#:~:text=in the ocean.-,The ocean holds about 97 percent of the Earth’s water,of water on the planet. [Accessed: 20-Feb-2020].

[11] Y. Wehbe *et al.*, “Analysis of an extreme weather event in a hyper-arid region using WRF-Hydro coupling, station, and satellite data,” *Nat. Hazards Earth Syst. Sci.*, 2019.

[12] L. M. G. Kurt Schwabe, Jose Albiac, Jeffery D. Connor, Rashid M. Hasan, *Drought in Arid and Semi-Arid Regions*. 2013.

[13] N. W. Arnell, “Climate change and global water resources,” in *Global Environmental Change*, 1999.

[14] World Water Assessment Programme (WWAP), “The United Nations World Water Development Report 2015: Water for a Sustainable World, Facts and Figures,” *UN Water Rep.*, 2015.

[15] P. H. Kirshen and K. M. Strzepek, “Comprehensive assessment of the freshwater resources of the world,” in *Proceedings, Congress of the International Association of Hydraulic Research, IAHR*, 1997.

[16] Howard S. Weater and Radvan A. Al-Weshah, “Hydrology of wadi systems. IHP regional network on wadi hydrology in the Arab region,” *Technical Documents in Hydrology*. 2002.

[17] A. A. Murad, “An Overview of Conventional and Non-Conventional Water Resources in

Arid Region: Assessment and Constrains of the United Arab Emirates (UAE)," *J. Water Resour. Prot.*, 2010.

[18] Z. S. Rizk, "Water resources in the United Arab Emirates," *Dev. Water Sci.*, vol. 50, pp. 245–264, Jan. 2003.

[19] S. Mazroui, Alya Al and Farrah, "The UAE Seeks Leading Position in Global Rain Enhancement Research," 2017. [Online]. Available: https://www.journalofweathermodification.org/index.php/JWM/article/view/562. [Accessed: 01-Jul-2020].

[20] J. Joss, "Applications of Weather Radar Systems. A Guide to Users of Radar Data in Meteorology and Hydrology. Edited by C. G. Collier. Co-ordinating Editors: J. W. Mason and D. R. Slogget. Ellis Horwood Limited Publisher, Chichester. 1989. Pp. 294. £44.50," *Q. J. R. Meteorol. Soc.*, 1990.

[21] C. CG, *Applications of weather radar systems. In A guide to uses of radar data in meteorology and hydrology*, Second Edi. Wiley-Praxis: Chichester, 1996.

[22] T. D. Mitchell and P. D. Jones, "An improved method of constructing a database of monthly climate observations and associated high-resolution grids," *Int. J. Climatol.*, 2005.

[23] P. Joyce, R.J.; Janowiak, J.E.; Arkin, P.A.; Xie, "CMORPH: A method that produces global precipitation estimates from passive microwave and infrared data at high spatial and temporal resolution," *Hydrometeorology*, vol. 5, pp. 487–503, 2004.

[24] and S. S. Nguyen, P., E.J. Shearer, H. Tran, M. Ombadi, N. Hayatbini, T. Palacios, P. Huynh, G. Updegraff, K. Hsu, B. Kuligowski, W.S. Logan, "The CHRS Data Portal, an easily accessible public repository for PERSIANN global satellite precipitation data," *Nat. Sci. Data*, vol. Vol. 6, Ar, 2019.

[25] U. Schneider, A. Becker, P. Finger, A. Meyer-Christoffer, B. Rudolf, and M. Ziese, "GPCC Full Data Reanalysis Version 7.0 at 0.5°: Monthly Land-Surface Precipitation from Rain-Gauges built on GTS-based and Historic Data," 2015.

[26] G. J. Huffman *et al.*, "NASA Global Precipitation Measurement (GPM) Integrated Multi-satellitE Retrievals for GPM (IMERG)," *Algorithm Theor. Basis Doc.*, 2018.

[27] E. F. Hu man, G.J.; Bolvin, D.T.; Nelkin, E.J.; Wol , D.B.; Adler, R.F.; Gu, G.; Hong, Y.; Bowman, K.P.; Stocker, "The TRMM multisatellite precipitation analysis (TMPA): Quasi-global, multiyear, combined-sensor precipitation estimates at fine scales," *Hydrometeorology*, vol. 8, pp. 38–55, 2007.

[28] Y. Wehbe, D. Ghebreyesus, M. Temimi, A. Milewski, and A. Al Mandous, "Assessment of the consistency among global precipitation products over the United Arab Emirates," *J. Hydrol. Reg. Stud.*, vol. 12, pp. 122–135, Aug. 2017.

[29] B. M. Fekete, C. J. Vörösmarty, J. O. Roads, and C. J. Willmott, "Uncertainties in precipitation and their impacts on runoff estimates," *J. Clim.*, 2004.

[30] Y. Yang and Y. Luo, "Evaluating the performance of remote sensing precipitation products CMORPH, PERSIANN, and TMPA, in the arid region of northwest China," *Theor. Appl. Climatol.*, 2014.

[31] M. Almazroui, "Calibration of TRMM rainfall climatology over Saudi Arabia during 1998-2009," *Atmos. Res.*, 2011.

[32] M. T. Mahmoud, M. A. Hamouda, and M. M. Mohamed, “Spatiotemporal evaluation of the GPM satellite precipitation products over the United Arab Emirates,” *Atmos. Res.*, vol. 219, pp. 200–212, May 2019.

[33] D. R. Chow, V. T., Mays, L., & Maidment, “Applied hydrology,” *Tata McGraw-Hill Educ.*, 1988.

[34] G. Devia, G. K., Ganasri, B., & Dwarakish, “A review on hydrological models,” *Aquat. Procedia*, vol. 4, pp. 1001–1007, 2015.

[35] M. Jajarmizadeh, M., Harun, S., & Salarpour, “A review on theoretical consideration and types of models in hydrology,” *J. Environ. Sci. Technol.*, vol. 5, no. 5, pp. 249–261, 2012.

[36] R. Shaw, E. M., Beven, K. J., Chappell, N. A., & Lamb, “Hydrology in practice,” *CRC Press.*, 2010.

[37] J. Cunderlik, “Hydrologic model selection for the CFCAS project: assessment of water resources risk and vulnerability to changing climatic conditions,” *Dep. Civ. Environ. Eng. Univ. West. Ontario.*, 2003.

[38] KJ Beven, *Rainfall-runoff Modelling: the primer*, vol. Second edi. John Wiley and Sons, 2011.

[39] G. Ghaffari, “The impact of DEM resolution on runoff and sediment modelling results,” *Res. J. Environ. Sci.*, vol. 5, no. 8, p. 691, 2011.

[40] C. –. Xu, “Hydrologic models,” *Textb. Uppsala Univ. Dep. Earth Sci. Hydrol.*, 2002.

[41] J. R. Arnold, J. G., Srinivasan, R., Muttiah, R. S., & Williams, “Large area hydrologic modeling and assessment part I: model development,” *JAWRA J. Am. Water Resour. Assoc.*, vol. 34, no. 1, pp. 73–89, 1998.

[42] B. Scharffenberg, M. Bartles, T. Brauer, M. Fleming, and G. Karlovits, “Hydrologic Modeling System HEC-HMS User’s Manual,” 2018.

[43] A. Bhuiyan, H. A., McNairn, H., Powers, J., & Merzouki, “Application of HEC-HMS in a Cold Region Watershed and Use of RADARSAT-2 Soil Moisture in Initializing the Model.,” *Hydrology*, vol. 4, no. 1, p. 9, 2017.

[44] B. McEnroe, “Guidelines for continuous simulation of streamflow in Johnson County, Kansas, with HEC-HMS,” *Dep. Civil, Environ. Archit. Eng. Univ. Kansas.*, 2010.

[45] P. Meenu, R., Rehana, S., & Mujumdar, “Assessment of hydrologic impacts of climate change in Tunga–Bhadra river basin, India with HEC-HMS and SDSM,” *Hydrol. Process.*, vol. 27, no. 11, pp. 1572–1589, 2013.

[46] W. R. Hamon, “Computation of direct runoff amounts from storm rainfall,” *General Assembly of Berkeley, Symposium on Surface Waters*. 1964.

[47] R. Saavedra, I., Lopez, J.L., Garcia-Martinez, “Dynamic wave study of flow in tidal channel system of San Juan River,” *J. Hydraul. Eng*, vol. 129, no. 7, pp. 519–526, 2003.

[48] S. Hu, H., Kreymborg, L., Doeing, B., Baron, K., & Jutila, “Gridded snowmelt and rainfall-runoff CWMS hydrologic modeling of the Red River of the North Basin,” *Hydrol. Eng.*, no. March/April, pp. 91–100, 2006.

[49] M. M. Sherif, M. M. Mohamed, A. Shetty, and M. Almulla, “Rainfall-runoff modeling of three wadis in the northern area of UAE,” *J. Hydrol. Eng.*, 2010.

[50] M. Temimi *et al.*, “Assessing The Impact of Changes in Land Surface Conditions on WRF Predictions in Arid Regions,” *J. Hydrometeorol.*, 2020.

[51] K. M. G. and A. R. F. R J Thomas, D I Schofield, *Geology of the Fujairah, United Arab Emirates (unpublished)*. Ministry of Energy, United Arab Emirates, 2006.

[52] N. R. Nelli *et al.*, “Micrometeorological measurements in an arid environment: Diurnal characteristics and surface energy balance closure,” *Atmos. Res.*, 2020.

[53] D. F. Steinhoff *et al.*, “Influences of the monsoon trough and Arabian heat low on summer rainfall over the United Arab Emirates,” *Mon. Weather Rev.*, 2018.

[54] T. Schwitalla, O. Branch, and V. Wulfmeyer, “Sensitivity study of the planetary boundary layer and microphysical schemes to the initialization of convection over the Arabian Peninsula,” *Q. J. R. Meteorol. Soc.*, 2020.

[55] M. Sherif, S. Akram, and A. Shetty, “Rainfall analysis for the Northern Wadis of United Arab Emirates: A case study,” *J. Hydrol. Eng.*, 2009.

[56] I. center for B. A. Emirate Soil Musium, “UAE soil Map,” 2016. [Online]. Available: https://www.emiratessoilmuseum.org/uae-soil-map. [Accessed: 19-Jun-2020].

[57] U. M. of Energy, “Ham Dam.” [Online]. Available: https://gis.moei.gov.ae/dams/pdfs/Ham.pdf%0A. [Accessed: 30-Jun-2020].

[58] Metrology Department, “Data sheet for the climate of UAE,” *ministry of Economics,AbuDhabi,UAE*, 2007. .

[59] G. A. Al-Rawas and C. Valeo, “Relationship between wadi drainage characteristics and peak-flood flows in arid northern oman,” *Hydrol. Sci. J.*, 2010.

[60] K. Renard and R. Keppel, “Hydrographs of Ephemeral Streams in the Southwest,” *J. Hydraul. Div.*, 1966.

[61] I. Cordery, D. H. Pilgrim, and D. G. Doran, “SOME HYDROLOGICAL CHARACTERISTICS OF ARID WESTERN NEW SOUTH WALES.,” in *National Conference Publication - Institution of Engineers, Australia*, 1983.

[62] M. O. Walters, “Transmission losses in arid region,” *J. Hydraul. Eng.*, 1990.

[63] D. A. Hughes and K. Sami, “Transmission losses to alluvium and associated moisture dynamics in a semiarid ephemeral channel system in Southern Africa,” *Hydrol. Process.*, 1992.

[64] A. Al-Qurashi, N. McIntyre, H. Wheater, and C. Unkrich, “Application of the Kineros2 rainfall-runoff model to an arid catchment in Oman,” *J. Hydrol.*, 2008.

[65] USGS EROS Archive, “Shuttle Radar Topography Mission (SRTM) 1 Arc-Second Global,” 2008. [Online]. Available: https://www.usgs.gov/centers/eros/science/usgs-eros-archive-digital-elevation-shuttle-radar-topography-mission-srtm-1-arc?qt-science_center_objects=0#qt-science_center_objects. [Accessed: 18-Mar-2020].

[66] G. J. Huffman *et al.*, “Algorithm Theoretical Basis Document (ATBD) Version 06 NASA Global Precipitation Measurement (GPM) Integrated Multi-satellitE Retrievals for GPM (IMERG),” *Natl. Aeronaut. Sp. Adm.*, 2019.

[67] C. Huang, Y. Chen, S. Zhang, and J. Wu, “Detecting, Extracting, and Monitoring Surface Water From Space Using Optical Sensors: A Review,” *Rev. Geophys.*, 2018.

[68] T. D. Acharya, D. H. Lee, I. T. Yang, and J. K. Lee, “Identification of water bodies in a landsat 8 OLI image using a J48 decision tree,” *Sensors (Switzerland)*, 2016.

[69] Y. Li, X. Gong, Z. Guo, K. Xu, D. Hu, and H. Zhou, “An index and approach for water extraction using Landsat–OLI data,” *Int. J. Remote Sens.*, 2016.

[70] Z. Liu, Z. Yao, and R. Wang, “Assessing methods of identifying open water bodies using Landsat 8 OLI imagery,” *Environ. Earth Sci.*, 2016.

[71] K. Singh, M. Ghosh, and S. R. Sharma, “WSB-DA: Water Surface Boundary Detection Algorithm Using Landsat 8 OLI Data,” *IEEE J. Sel. Top. Appl. Earth Obs. Remote Sens.*, 2016.

[72] H. Xie, X. Luo, X. Xu, H. Pan, and X. Tong, “Evaluation of Landsat 8 OLI imagery for unsupervised inland water extraction,” *Int. J. Remote Sens.*, 2016.

[73] Y. Yang *et al.*, “Landsat 8 OLI image based terrestrial water extraction from heterogeneous backgrounds using a reflectance homogenization approach,” *Remote Sens. Environ.*, 2015.

[74] I. J. Barton and J. M. Bathols, “Monitoring floods with AVHRR,” *Remote Sens. Environ.*, 1989.

[75] Y. Chen, C. Huang, C. Ticehurst, L. Merrin, and P. Thew, “An evaluation of MODIS daily and 8-day composite products for floodplain and wetland inundation mapping,” *Wetlands*, 2013.

[76] D. Peng, L. Xiong, S. Guo, and N. Shu, “Study of Dongting Lake area variation and its influence on water level using MODIS data,” *Hydrol. Sci. J.*, 2005.

[77] C. Huang, Y. Chen, J. Wu, L. Li, and R. Liu, “An evaluation of Suomi NPP-VIIRS data for surface water detection,” *Remote Sens. Lett.*, 2015.

[78] R. Andreoli, H. Yésou, J. Li, and Y. L. Desnos, “Inland lake monitoring using low and medium resolution ENVISAT ASAR and optical data: Case study of Poyang Lake (Jiangxi, P.R. China),” in *International Geoscience and Remote Sensing Symposium (IGARSS)*, 2007.

[79] S. C. J. Palmer, T. Kutser, and P. D. Hunter, “Remote sensing of inland waters: Challenges, progress and future directions,” *Remote Sensing of Environment*. 2015.

[80] S. K. McFeeters, “Using the normalized difference water index (ndwi) within a geographic information system to detect swimming pools for mosquito abatement: A practical approach,” *Remote Sens.*, 2013.

[81] Q. Guo, X. Wu, X. Sang, Y. Fu, Y. Zang, and X. Gong, “An integrated study on change detection and environment evaluation of surface water,” *Appl. Water Sci.*, 2020.

[82] Landsat 8 OLI/TIRS, “Landsat Science.” [Online]. Available: Landsat 8 OLI/TIRS Digital Object Identifier (DOI) number: /10.5066/F71835S6. [Accessed: 13-Mar-2020].

[83] K. Rokni, A. Ahmad, A. Selamat, and S. Hazini, “Water feature extraction and change detection using multitemporal landsat imagery,” *Remote Sens.*, 2014.

[84] D. T. Ghebreyesus, M. Temimi, A. Fares, and H. K. Bayabil, “A multi-satellite approach for water storage monitoring in an arid watershed,” *Geosci.*, 2016.

[85] S. Lu, N. Ouyang, B. Wu, Y. Wei, and Z. Tesemma, “Lake water volume calculation with time series remote-sensing images,” *Int. J. Remote Sens.*, 2013.

[86] Z. Du *et al.*, “Estimating surface water area changes using time-series Landsat data in the Qingjiang River Basin, China,” *J. Appl. Remote Sens.*, 2012.

[87] Z. Tang, W. Ou, Y. Dai, and Y. Xin, “Extraction of water body based on LandSat TM5 imagery - A case study in the Yangtze River,” in *IFIP Advances in Information and Communication Technology*, 2013.

[88] H. M. El-Asmar and M. E. Hereher, “Change detection of the coastal zone east of the Nile Delta using remote sensing,” *Environ. Earth Sci.*, 2011.

[89] L. E. Reinelt, J. Velikanje, and E. J. Bell, “Development and application of a geographic information system for wetland/watershed analysis,” *Comput. Environ. Urban Syst.*, 1991.

[90] R. Jayakrishnan, R. Srinivasan, C. Santhi, and J. G. Arnold, “Advances in the application of the SWAT model for water resources management,” *Hydrol. Process.*, 2005.

[91] P. H. Martin, E. J. LeBoeuf, J. P. Dobbins, E. B. Daniel, and M. D. Abkowitz, “Interfacing GIS with water resource models: A state-of-the-art review,” *Journal of the American Water Resources Association*. 2005.

[92] J. E. Nash and J. V. Sutcliffe, “River flow forecasting through conceptual models part I - A discussion of principles,” *J. Hydrol.*, 1970.

[93] K. Beven, “Prophecy, reality and uncertainty in distributed hydrological modelling,” *Adv. Water Resour.*, 1993.

[94] A. J. Jakeman and G. M. Hornberger, “How much complexity is warranted in a rainfall-runoff model?,” *Water Resour. Res.*, 1993.

[95] P. C. Young and K. J. Beven, “Data-based mechanistic modelling and the rainfall-flow non-linearity,” *Environmetrics*, 1994.

[96] N. McIntyre and A. Al-Qurashi, “Performance of ten rainfall-runoff models applied to an arid catchment in Oman,” *Environ. Model. Softw.*, 2009.

[97] V. P. Singh, “Kinematic wave modelling in water resources: A historical perspective,” *Hydrol. Process.*, 2001.

[98] T. A. Schroeder, W. B. Cohen, C. Song, M. J. Canty, and Z. Yang, “Radiometric correction of multi-temporal Landsat data for characterization of early successional forest patterns in western Oregon,” *Remote Sens. Environ.*, 2006.

[99] Landsat8, “Landsat 8 Data user manual.” [Online]. Available: https://www.usgs.gov/land-resources/nli/landsat/using-usgs-landsat-level-1-data-product. [Accessed: 13-Mar-2020].

[100] P. S. Chavez Jr., “Image-based atmospheric corrections - Revisited and improved,” *Photogramm. Eng. Remote Sensing*, 1996.

[101] R. T. Brooks and M. Hayashi, “Depth-area-volume and hydroperiod relationships of ephemeral (vernal) forest pools in Southern New England,” *Wetlands*, 2002.

[102] C. Medina, J. Gomez-Enri, J. J. Alonso, and P. Villares, “Water volume variations in Lake Izabal (Guatemala) from in situ measurements and ENVISAT Radar Altimeter (RA-2) and Advanced Synthetic Aperture Radar (ASAR) data products,” *J. Hydrol.*, 2010.

[103] S. K. McFeeters, “The use of the Normalized Difference Water Index (NDWI) in the delineation of open water features,” *Int. J. Remote Sens.*, 1996.

[104] H. Xu, “Modification of normalised difference water index (NDWI) to enhance open water features in remotely sensed imagery,” *Int. J. Remote Sens.*, 2006.

[105] W. J. Rawls, C. L. Brakensiek, and K. E. Saxton, “Estimation of soil water properties.,” *Trans. - Am. Soc. Agric. Eng.*, 1982.

[106] B. K. Nyarko, “Flood risk zoning of Ghana: Accra experience,” in *International Archives of the Photogrammetry, Remote Sensing and Spatial Information Sciences - ISPRS Archives*, 2000.

[107] C. Y. Xu, “Modelling the effects of climate change on water resources in central Sweden,” *Water Resour. Manag.*, 2000.

[108] H. De Moel, J. Van Alphen, and J. C. J. H. Aerts, “Flood maps in Europe - Methods, availability and use,” *Nat. Hazards Earth Syst. Sci.*, 2009.

[109] P. D. Bates and A. P. J. De Roo, “A simple raster-based model for flood inundation simulation,” *J. Hydrol.*, 2000.

[110] J. Y. & A. P. J. D. R. J. M. Van Der Knijff, “LISFLOOD: a GIS-based distributed model for river basin scale water balance and flood simulation,” *Int. J. Geogr. Inf. Sci.*, vol. 24(2), pp. 189–212, 2010.

[111] J. M. Hamrick, “A Three-Dimensional Environmental Fluid Dynamics Computer Code: Theoretical and Computational Aspects,” *Coll. William Mary, Virginia Inst. Mar. Sci. Spec. Rep. 317, 63 pp.*, 1992.

[112] Deltares, “SOBEK Suite,” *2011*. [Online]. Available: https://www.deltares.nl/nl/software/sobek-suite/#features. [Accessed: 04-Jul-2020].

[113] D. H. Institute, “MIKE-SHE,” 2016. [Online]. Available: https://www.mikepoweredbydhi.com/products/mike-she. [Accessed: 21-Jun-2020].

[114] H. C. Yeh, G.T.; Huang, G.B.; Zhang, F.; Cheng, H.P.; Lin, “WASH123D: A Numerical Model of Flow, Thermal Transport, and Salinity, Sediment, and Water Quality Transport in WAterSHed Systems of 1-D Streamriver Network, 2-D Overland Regime, and 3-D Subsurface Media,” *Tech. Rep. Submitt. To EPA; Dep. Civ. Environ. Eng. Univ. Cent. Florida Orlando, FL, USA*, 2006.

[115] R. K. Price and P. G. Samuels, “COMPUTATIONAL HYDRAULIC MODEL FOR RIVERS.,” *Proc. Inst. Civ. Eng. (London). Part 1 - Des. Constr.*, 1980.

[116] B. Gary W, “HEC-RAS River Analysis System: user Manual 1D and 2D,” *Inst. Water Resour. Hydrol. Eng. Cent.*, 2016.

[117] T. V. Hromadka and C. C. Yen, “A diffusion hydrodynamic model (DHM),” *Adv. Water Resour.*, 1986.

[118] K. Feng and F. J. Molz, “A 2-D, diffusion-based, wetland flow model,” *J. Hydrol.*, 1997.

[119] D. R. & S. A. Maidment, “Introduction to HEC – RAS: CE 394k.2 Surface Water hydrology, electronic document,” 1999. [Online]. Available: http://www.ce.utexas.edu/prof/maidment/grad/tate/research/RASExercise/webfiles/hecras.html. [Accessed: 12-Feb-2019].

[120] M. Salajegheh, A., Bakhshaei, M., Chavoshi, S., Keshtkar, A. R., & Najafi Hajivar, “Floodplain mapping using HEC-RAS and GIS in semi-arid regions of Iran,” *Desert*, vol.

14, no. 1, pp. 83–93, 2009.

[121] M. S. Khattak, F. Anwar, T. U. Saeed, M. Sharif, K. Sheraz, and A. Ahmed, “Floodplain Mapping Using HEC-RAS and ArcGIS: A Case Study of Kabul River,” *Arab. J. Sci. Eng.*, 2016.

[122] V. M. Quirogaa, S. Kurea, K. Udoa, and A. Manoa, “Application of 2D numerical simulation for the analysis of the February 2014 Bolivian Amazonia flood: Application of the new HEC-RAS version 5,” *Ribagua*, 2016.

[123] I. Shustikova, A. Domeneghetti, J. C. Neal, P. Bates, and A. Castellarin, “Comparing 2D capabilities of HEC-RAS and LISFLOOD-FP on complex topography,” *Hydrol. Sci. J.*, 2019.

[124] J. O. Okirya Martin, Albert Rugumayo, “APPLICATION OF HEC HMS/RAS AND GIS TOOLS IN FLOOD MODELING: A CASE STUDY FOR RIVER SIRONKO – UGANDA,” *Glob. J. Eng. Des. Technol.*, vol. 1(2), pp. 19–31, 2012.

[125] L. Deng, M. F. Mccabe, G. Stenchikov, J. P. Evans, and P. A. Kucera, “Simulation of flash-flood-producing storm events in Saudi Arabia using the weather research and forecasting model,” *J. Hydrometeorol.*, 2015.

[126] M. Al-Zahrani, A. Al-Areeq, and H. Sharif, “Flood analysis using HEC-RAS model: A case study for Hafr Al-Batin, Saudi Arabia,” in *E3S Web of Conferences*, 2016.

[127] A. Ezzine, S. Saidi, T. Hermassi, I. Kammessi, F. Darragi, and H. Rajhi, “Flood mapping using hydraulic modeling and Sentinel-1 image: Case study of Medjerda Basin, northern Tunisia,” *Egypt. J. Remote Sens. Sp. Sci.*, 2020.

[128] C. Popescu, “Theoretical background: Unsteady flow. In G. Di Baldassarre (Author),” in *Floods in a Changing Climate: Inundation Modelling (International Hydrology Series*, Cambridge: Cambridge University Press., 2012, pp. 21–30.

[129] P. Fan and J. C. Li, “Diffusive wave solutions for open channel flows with uniform and concentrated lateral inflow,” *Adv. Water Resour.*, 2006.

[130] B. C. Yen, “OPEN-CHANNEL FLOW EQUATIONS REVISITED.,” *ASCE J Eng Mech Div*, 1973.

[131] V. T. Chow, *Open-Channel Hydraulics. Ven Te Chow. McGraw-Hill, New York, 1959. xviii + 680 pp. Illus. $17*. 1959.

[132] V. Te Chow, D. R. Maidment, and L. W. Mays, *Applied hydrology (letters)*. 1988.

[133] V. M. Ponce, R. M. Li, and D. B. Simons, “APPLICABILITY OF KINEMATIC AND DIFFUSION MODELS,” *ASCE J Hydraul Div*, 1978.

[134] L. Cozzolino *et al.*, “Exact solution of the dam-break problem for constrictions and obstructions in constant width rectangular channels,” *J. Hydraul. Eng.*, 2017.

[135] V. K. Sridharan, S. G. Monismith, D. A. Fong, and J. L. Hench, “One-dimensional particle tracking with streamline preserving junctions for flows in channel networks,” *J. Hydraul. Eng.*, 2018.

[136] L. P. Chamorro and F. Porté-Agel, “Channel bed slope effect on the height of gravity waves produced by a sudden downstream discharge stoppage,” *J. Hydraul. Eng.*, 2010.

[137] B. C. Yen and C. S. Tsai, “On noninertia wave versus diffusion wave in flood routing,” *J.*

Hydrol., 2001.

[138] M. M. Morsy *et al.*, "A cloud-based flood warning system for forecasting impacts to transportation infrastructure systems," *Environ. Model. Softw.*, 2018.

[139] J. T. S. Savage, P. Bates, J. Freer, J. Neal, and G. Aronica, "When does spatial resolution become spurious in probabilistic flood inundation predictions?," *Hydrol. Process.*, 2016.

[140] T. H. . Haile, A.T. and Rientjes, "Effects of LiDAR DEM resolution in flood modelling. A model sensitivity study for the city of Tegucigalpa, Honduras," *ISPRS WG*, vol. 3, pp. 12–14, 2005.

[141] T. J. Fewtrell, P. D. Bates, M. Horritt, and N. M. Hunter, "Evaluating the effect of scale in flood inundation modelling in urban environments," *Hydrol. Process.*, 2008.

[142] L. . Chow, V.T.; Maidment, D.R.; Mays, *Applied Hydrology*. McGraw-Hill Book Co., New York, 1988.

[143] R. . McCuen, *Hydrologic Analysis and Design*, 2nd editio. Prentice Hall, New Jersey, 1998.

[144] D. S.-M. and M. A. Friedl, "MODIS Land Cover (MCD12Q1 and MCD12C1) Product," 2018.

[145] MLIT, "Flood hazard mapping manual in Japan," *Minist. L. Infrastruct. Transp.*, p. 87, 2005.

[146] and D. S. Policelli, F., "NRT Global Flood Mapping," *NASA*, 2017. [Online]. Available: https://floodmap.modaps.eosdis.nasa.gov. [Accessed: 26-Mar-2020].

[147] A. B. Carroll, M. L., DiMiceli, C.M., Townshend, J.R.G., Sohlberg, R.A., Hubbard and M. R. Wooten, "MOD44W: Global MODIS water maps user guide," 2017. [Online]. Available: https://lpdaac.usgs.gov/documents/109/MOD44W_User_Guide_ATBD_V6.pdf. [Accessed: 21-Mar-2020].

[148] H. Tran, P. H. U. Nguyen, M. Ombadi, K. Hsu, S. Sorooshian, and K. Andreadis, "Improving hydrologic modeling using cloud-free modis flood maps," *J. Hydrometeorol.*, 2019.

[149] and R. W. Vermote, E., "MOD09GA MODIS/Terra Surface Reflectance Daily L2G Global 1km and 500m SIN Grid V006," *NASA EOSDIS LP DAAC*, 2015.

[150] J. R. McCollum, A. Gruber, and M. B. Ba, "Discrepancy between gauges and satellite estimates of rainfall in equatorial Africa," *J. Appl. Meteorol.*, 2000.

[151] S. E. Nicholson *et al.*, "Validation of TRMM and other rainfall estimates with a high-density gauge dataset for West Africa. Part II: Validation of TRMM rainfall products," *J. Appl. Meteorol.*, 2003.

[152] E. Tarnavsky, M. Mulligan, and G. Husak, "Spatial disaggregation and intensity correction of TRMM-based rainfall time series for hydrological applications in dryland catchments," *Hydrol. Sci. J.*, 2012.

[153] R. BERNDTSSON, "Spatial and temporal variability of rainfall and potential evaporation in Tunisia," *IAHS-AISH Publ.*, 1987.

[154] P. López López, W. W. Immerzeel, E. A. Rodríguez Sandoval, G. Sterk, and J. Schellekens, "Spatial downscaling of satellite-based precipitation and its impact on

discharge simulations in the magdalena river basin in Colombia," *Front. Earth Sci.*, 2018.

[155] C. Chen, S. Zhao, Z. Duan, and Z. Qin, "An Improved Spatial Downscaling Procedure for TRMM 3B43 Precipitation Product Using Geographically Weighted Regression," in *IEEE Journal of Selected Topics in Applied Earth Observations and Remote Sensing*, 2015.